Nanocellulose-assisted preparation of electromagnetic interference shielding materials with diversified microstructure

Review Article

Author(s):
Zeng, Zhihui; Qiao, Jing; Zhang, Runa; Liu, Jiurong; Nyström, Gustav (iD)

REVIEW

SmartMat WILEY

Nanocellulose-assisted preparation of electromagnetic interference shielding materials with diversified microstructure

Zhihui Zeng[1] | **Jing Qiao**[2] | **Runa Zhang**[1] | **Jiurong Liu**[1] | **Gustav Nyström**[3,4]

[1]Key Laboratory for Liquid-Solid Structural Evolution and Processing of Materials, School of Materials Science and Engineering, Shandong University, Jinan, China

[2]School of Mechanical Engineering, Shandong University, Jinan, China

[3]Laboratory for Cellulose and Wood Materials, Swiss Federal Laboratories for Materials Science and Technology (Empa), Dübendorf, Switzerland

[4]Department of Health Sciences and Technology, ETH Zürich, Zürich, Switzerland

Correspondence
Zhihui Zeng and Jiurong Liu,
Key Laboratory for Liquid-Solid
Structural Evolution and Processing of
Materials, School of Materials Science and
Engineering, Shandong University,
250061 Jinan, China.
Email: zhihui.zeng@sdu.edu.cn and
jrliu@sdu.edu.cn

Gustav Nyström, Laboratory for Cellulose
and Wood Materials, Swiss Federal
Laboratories for Materials Science and
Technology (Empa), 8600 Dübendorf,
Switzerland.
Email: gustav.nystroem@empa.ch

Abstract

Sustainable and renewable nanocellulose attracts more and more attention in various fields due to its high strength-to-weight ratio, small diameter, large aspect ratio, and abundant functional groups. The excellent properties and structural characteristics enabled a great potential of nanocellulose for efficient interactions with functional nanomaterials such as carbon nanotube, graphene, transition metal carbides/nitrides (MXenes), and metal nanoparticles, which is beneficial for preparing high-performance electromagnetic interference (EMI) shields. We review the advances in the nanocellulose-assisted preparation of composite films and aerogels for EMI shielding application. The nanocellulose-based composites are evaluated in terms of their EMI shielding performance and the shielding mechanisms, including conduction, polarization, and multiple reflections are summarized. In addition to the constituent structure and contents, we highlight the significance of the microstructure design in enhancing the EMI shielding performance of the nanocellulose-based EMI shields. Finally, the current challenges and outlook for these fascinating nanocellulose-based EMI shielding composites are discussed.

KEYWORDS
aerogels, electromagnetic interference shielding, film, microstructure design, nanocellulose, nanocomposite

1 | INTRODUCTION

With the rapid development of the electronic industry and communication technology, associated electromagnetic radiation or pollution issues have been receiving increasing attention. Interfering electromagnetic waves (EMWs) or radiation not only disrupt the normal operation of electronics itself but also have potential influences on the human health.[1–6] Traditional metal shields are efficient but suffer from high density, poor mechanical flexibility, undesirable corrosion susceptibility, and difficult processability, restricting the applications for next-generation electromagnetic interference (EMI) shields.[7–11] High-performance EMI shielding materials with low density and thickness, good mechanical strength and flexibility, easy processing characteristics, and high and controllable EMI shielding effectiveness (SE) are highly demanded.[12–17] Recently, conductive polymer nanocomposites (CPCs) integrated with functional nanomaterials such as carbon nanotubes (CNTs),[8,18–27] graphene,[28–36] transition metal carbides and/or nitrides (MXenes),[37–50] and metal nanoparticles[51–56] have been considered as promising EMI shielding materials due to advantages in low mass density, chemical stability, and design flexibility. These functional nanomaterials with excellent mechanical properties can have a large aspect ratio and remarkable electrical conductivities, which is beneficial for forming efficient conductive paths in the CPCs.[31,57–62] Combined with the generated interfaces between the nanomaterials and polymers, which can contribute to the interfacial polarization loss of incident EMWs, the CPCs can show high EMI shielding performance.[63–70] In addition to the control of constituents and contents of the functional nanomaterials for adjusting the EMI shielding performance of the CPCs, the microstructure design is vital for achieving high-performance, controllable EMI shields. Nowadays, one efficient design strategy focuses on introducing more interior surfaces/interfaces in the CPCs. Numerous interior surfaces/interfaces can increase the multiple reflections or scattering of incident EMWs, increasing the interactions of functional constituents and EMWs.[71–74] In combination with the considerable EMW loss ability with the constituents, the EMI shielding performance can be enhanced. This means that the porous structure introduced in the shields not only further reduces the weight but also leads to enhanced EMI SE of the aerogel-based shields in comparison to the bulk counterpart.[75,76] Compressing the composite aerogels to exclude the micrometer-sized pores can reduce the EMI SE, further implying the positive influence of the porous structure on the EMI shielding performance.[77–80] A rational design of the constituents and microstructure for improving the EMI shielding performance of the CPCs and further advancing the understanding of the structure–property relationships is the key to developing high-performance EMI shielding materials to satisfy various application scenarios. However, the challenges still focus on the processing and full utilization of the functional nanomaterials and the high-efficiency design of microstructure. Moreover, petrochemical building units or polymers usually employed in the composition of the EMI shields are often not sustainable, further hindering the application potential. Efficiently utilizing the building units via a sustainable and renewable way to fabricate high-performance EMI shields associated with minimizing the impacts on the environment remains crucial.

Nanocellulose such as cellulose nanofibrils/nanofibers (CNFs) or cellulose nanocrystals, made up of cellulose, which is the most abundant renewable polymer on earth, has attracted more and more attention in recent years for widespread applications, including packing, energy storage, strain/pressure sensing, thermal insulation, oil/water separation, flexible devices, and EMI shields.[81–87] Given the high strength-to-weight ratio, small diameter, large aspect ratio and specific surface area, and abundant hydrophilic functional groups (e.g., –OH and –COOH), the nanocellulose promised good dispersibility and efficient interactions with the functional nanomaterials, thereby enabling a facile construction of macrostructures.[88–93] The presence of amphiphilic faces derived from the different crystal planes of the nanocellulose in combination with the functional groups allows these materials to act as green, stable, and low-cost dispersants.[89,94,95] This enables a homogeneous mixing of nanocellulose and inherently inert functional nanomaterials without additional surfactants or chemical functionalization. Furthermore, the excellent mechanical properties and large aspect ratio of the renewable nanocelluloses were also instrumental in the preparation of robust biopolymer-based composite films or aerogels, as the nanocellulose can efficiently support or bind the functional nanomaterials with otherwise poor interfacial interaction or gelation capability. Such composites could have extensive functional applications because nanocellulose could be easily integrated with various versatile nanomaterials. Furthermore, a unique structure-directing function of nanocellulose, derived from the small diameter, good mechanical properties, and strong tendency to form lamellar film, contributed to the preparation of thin yet robust composite films or low-density, stable composite aerogels with ordered cell walls.[96–98] This thus enabled the build-up of function-targeted composites with minimum material consumption and good structural stability, which was important for the development of lightweight EMI shielding architectures. Until now, several

researchers have reported on nanocellulose covering the material preparation, production, processing, characterization strategies, surface functionalization, and application fields because of the excellent material properties and broad application potential.[99–116] Particularly, the merits of nanocellulose lead to a large potential for replacing conventional polymers in EMI shielding materials, and the corresponding reports are increasing year by year. In the whole EMI shielding field, the nanocellulose-based materials are still at an early stage, but the trend of rapid growth has been emerging. Therefore, a review of nanocellulose-assisted preparation of CPC-based EMI shielding architectures involving the constituent and microstructure design is highly desired. Such a report can advance the understanding of the structure–property relationships within these materials and further help to improve EMI shielding architectures in general.

Here, this review highlights the current status, ongoing challenges, and outlook of the nanocellulose-assisted EMI shielding nanocomposites in the forms of films and porous aerogels. In addition to the EMI shielding theory, mechanism, and measurements, we emphasize the vital roles that nanocellulose plays in constructing high-performance EMI shields with various structures (Figure 1).[89,117–119] We categorize the EMI shields into nanocellulose-based composite films with double-layer coating, alternating-layer, and "brick-and-mortar" structure and nanocellulose-based composite aerogels with random and aligned pore morphologies.

The outlook of the nanocellulose-based EMI shields is also discussed, providing a guideline for future developments of high-performance EMI shielding architectures.

2 | THEORY OF EMI SHIELDING PERFORMANCE

2.1 | Mechanism of EMI shielding performance

Nowadays, EMI shielding is regarded as the most flexible and efficient method to protect against electromagnetic pollution. The EMI shielding refers to utilizing shielding facilities to impede the propagation of EMWs and to eliminate interference with electronic components. According to the type of radiation source, the EMI shielding methods can be divided into electrostatic field shielding, magnetic field shielding, and electromagnetic field shielding. A Faraday cage cavity is usually utilized to shield the disturbance from electrostatic fields. Based on the electrostatic balance principle, a conductive cavity can be an equipotential body, within which the electric field intensity is zero.[120] In the case of magnetostatic or low-frequency magnetic field shielding, achieving the magnetic shielding is more significant because the field energy concentrates on the magnetic field. A low-reluctance cavity with high permeability (usually made by iron, cobalt, nickel, and their alloys) is highly desired. The cavity provides the magnetic bypass so that the
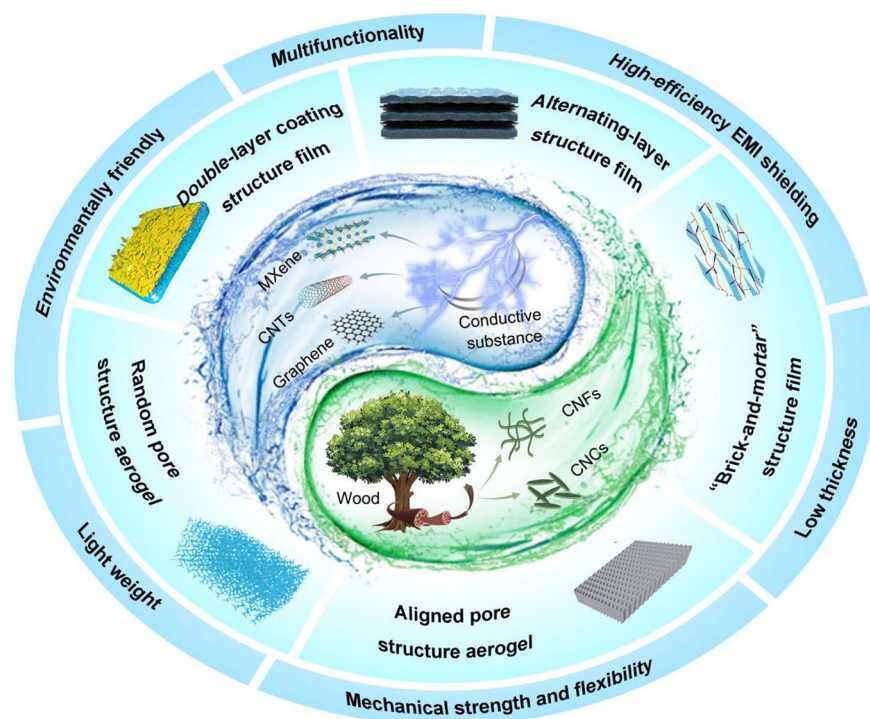

FIGURE 1 Schematic illustration of the nanocellulose-assisted preparation of composites for electromagnetic interference shielding application. Reproduced with permission: Copyright 2021, Elsevier,[117] Wiley,[89,118] and American Chemical Society.[119]

magnetic field tends to concentrate in the magnetic shells. As a result, the sensitive components inside the shielding cavity get the protection.[120] According to Maxwell's electromagnetic theory, the electric fields and magnetic fields are always intertwined with each other. Therefore, the electromagnetic field can be shielded by attenuating any one of them. In fact, research on the shielding for high-frequency alternating electromagnetic fields is more attractive, as they have a wider range of practical application scenarios. For example, technologically mature metal-plated fabrics mainly aim at the physical protection under strong electromagnetic radiation and the application of shielding anechoic chambers (0.1 MHz–3 GHz). Various high-conductivity shielding films/adhesive tapes point at the EMI shielding or electromagnetic compatibility between different electronic components in electronic communication equipment, such as cellphones, computers, and so on (0.5–100 GHz). Hence, the shielding mechanisms, methods, and research progress for high-frequency EMWs are the focus of this review.

As for the mechanism of EMI shielding, various theories have been proposed, including the transmission line theory, eddying effect theory, and the electromagnetic field theory. Among these, the transmission line theory is widely accepted. Accordingly, for a shielding medium with finite thickness, the incident EMWs can be divided into three parts: reflection, absorption, and transmission. Typically, when the EMWs impact the front surface, most of them are directly reflected due to the impedance mismatch between the air (or the free space) and the medium.[121] Some of the EMWs that still enter into the shielding materials are attenuated into heat, and the residual will penetrate the rear surface as transmitted waves.[122] Meanwhile, the EMWs inside the medium can be repeatedly reflected by the two outer surfaces or different internal layers/interfaces, which can result in multiple reflections and enhanced absorption. On the macroscopic level, generally, the EMI shielding materials possess abundant mobile charge carriers or electric/magnetic dipoles. The interaction between EMWs and the shielding medium can cause the charges or dipoles to be excited and redistributed, which form an opposing electromagnetic field to resist the external field.[123] The electric microcurrent produced by charge motion and the dipole polarization delaying the electromagnetic field can induce resistance/conductive loss and dielectric loss, resulting in the wave absorption. For magnetic shielding materials, various absorption/attenuation pathways such as magnetic domain resonance, hysteresis loss, and eddy current losses, should also be considered.

2.2 | Calculation of EMI shielding performance

The most direct indicator to evaluate the shielding ability of materials is EMI SE, which is expressed in decibels (dB). The EMI SE describes the intensity ratio of the incident field to the transmitted field and thus gives a measure of the attenuation of the field by the shielding material[124,125]:

$$\mathrm{SE} = 10\log\left(\frac{P_{\mathrm{inc}}}{P_{\mathrm{tra}}}\right) = 20\log\left(\frac{E_{\mathrm{inc}}}{E_{\mathrm{tra}}}\right) = 20\log\left(\frac{H_{\mathrm{inc}}}{H_{\mathrm{tra}}}\right), \tag{1}$$

where P, E, and H are the power density, electric field intensity, and magnetic field intensity, respectively, and the subscripts refer to the incident and transmitted waves, respectively.

Generally, high conductivity materials are most appropriate for EMI shielding. For the conductive substance, theoretically, the EMI SE value can be calculated by the Simon formalism as follows[126,127]:

$$\mathrm{SE} = 50 + 10\log\left(\frac{\sigma}{f}\right) + 1.7t\sqrt{\sigma f}, \tag{2}$$

where σ is the electrical conductivity, f is the EMW frequency, and t is the thickness of the shielding layer. This formula says that the EMI SE is positively related to the thickness and conductivity, and a better EMI SE can be more easily achieved at a higher frequency.

According to the transmission line theory (classical Schelkunoff theory), the EMI SE is the sum of the absorption loss (SE_A), reflection loss (SE_R), and multiple reflection loss (SE_M). Notably, the multiple reflections here correspond to that between the two interfaces of the shield (on the macroscopic scale) rather than that caused by the small interfaces/surfaces inside the materials. In the calculation, based on the law of power balance ($R + A + T = 1$), the EMI SE consists of the reflection of energy (also called shielding by reflection, $\mathrm{SE}_{R'}$) and absorption of energy (also called shielding by absorption, $\mathrm{SE}_{A'}$). The relationship can be described as follows[125]:

$$\mathrm{SE} = \mathrm{SE}_A + \mathrm{SE}_R + \mathrm{SE}_M = \mathrm{SE}_{A'} + \mathrm{SE}_{R'}. \tag{3}$$

The absorption loss (SE_A) of shielding materials has a positive correlation with the electrical conductivity and magnetic permeability, as well the wave frequency and the shield thickness, which can be expressed as follows[128]:

$$\mathrm{SE}_A = 20\log e \times t\sqrt{\frac{\omega\sigma_{\mathrm{r}}\mu_{\mathrm{r}}}{2}} = 20\log e \times \frac{t}{\delta}, \tag{4}$$

where ω is the angular frequency of the EMWs, σ_r refers to the relative electrical conductivity (the electrical conductivity relative to that of copper, 5.8×10^7 S/m), μ_r represents the relative magnetic permeability (magnetic permeability relative to that of the free space, $4\pi \times 10^{-7}$ H/m), δ is the skin depth, which means the distance from the surface to the depth that the electric/magnetic field intensity decreases to $1/e$ of initial values. The skin depth indicates that the EMW absorption can occur only in the superficial layer of the conductor, which is expressed as follows:

$$\delta = \sqrt{\frac{2}{\omega \sigma_r \mu_r}} = \frac{1}{\sqrt{\pi f \sigma_r \mu_r}}. \tag{5}$$

Similarly, the reflection loss (SE_R) of shielding materials is also affected by the electrical conductivity, magnetic permeability, and wave frequency, which can be described as follows[120]:

$$SE_R = 168.2 + 10 \log\left(\frac{\sigma_r}{f \mu_r}\right). \tag{6}$$

Besides, the multiple reflection loss (SE_M) of shielding materials can be calculated by the following equation[120,123]:

$$SE_M = 20 \log\left(1 - e^{-\frac{2t}{\delta}}\right) = 20 \log\left(1 - 10^{-\frac{SE_A}{10}}\right). \tag{7}$$

In this case, if the absorption shielding performance is much larger than 10 dB, or the material thickness is much larger than the skin depth, the influence of multiple reflections can be ignored. In the rest of this review, the multiple reflections specifically refer to those caused by the interior interfaces/surfaces inside the materials.

In the calculations, the reflection loss ($SE_{R'}$) and absorption loss ($SE_{A'}$) are defined as follows:

$$SE_{R'} = 10 \log\left|\frac{1}{1-R}\right| = 10 \log\left|\frac{1}{1-S_{11}^2}\right|, \tag{8}$$

$$SE_{A'} = 10 \log\left|\frac{1-R}{T}\right| = 10 \log\left|\frac{1-S_{11}^2}{S_{21}^2}\right|, \tag{9}$$

where S_{11} and S_{21} refer to the complex scattering parameters (S-parameters).

Based on these relations, it can be found that the EMI SE primarily depends on the conductivity of the shielding materials. Additionally, the shielding thickness also efficiently affects the absorption. In practical application,

increasing the thickness of shielding materials is regarded as the most simple and effective method to improve the EMI shielding performances. However, to meet the requirements of next-generation EMI shields, the development of lightweight EMI shielding materials with low density or thickness has always been an unremitting pursuit for researchers.

Therefore, to evaluate the comprehensive shielding performance by taking the density and thickness into consideration, the specific SE (SSE, defined as the ratio of EMI SE to density or thickness) and the surface SSE (SSE/t or SSE/d, defined as the EMI SE divided by the thickness and density of shields, namely, the ratio of EMI SE to the areal density $\rho_{\square}$) values are usually calculated as[11,12,128,129]

$$SSE = SE/\rho \quad (\text{usually for an aerogel}, dB \cdot cm^3/g) \tag{10}$$

or

$$SSE = SE/t \quad (\text{usually for a film}, dB/mm), \tag{11}$$

$$SSE/t = \frac{SE}{\rho_{\square}} = \frac{SE}{\rho t} \quad (dB \cdot cm^2/g). \tag{12}$$

2.3 | Measurement of EMI shielding performance

Generally, the far-field EMI SE of shielding properties is commonly calculated by the S-parameters (S_{11}, S_{21}, S_{22}, and S_{12}), which can be ascertained by the vector network analyzer. There are several methods to obtain the S-parameters, such as the open field method, shielded room method, coaxial transmission line method, and waveguide method. Among them, the waveguide method is most employed due to its flexibility and broad-frequency-range measurability (from 0.96 to 112 GHz). At this point, the X-band (8.2–12.4 GHz) is intensively studied because it is the common frequency range for communication applications. Typically, the shielding materials are shaped into a rectangular block/film (22.86 mm × 10.16 mm) to fill into the waveguide fixture. Based on the obtained S-parameters, the coefficients of absorption (A), reflection (R), transmission (T), and the EMI SE values can be calculated by the following equations[130,131]:

$$R = |S_{11}|^2 = |S_{22}|^2, \tag{13}$$

$$T = |S_{12}|^2 = |S_{21}|^2, \tag{14}$$

$$SE_T = 10 \log\left(\frac{1}{T}\right) = 10 \log\left(\frac{1}{|S_{12}|^2}\right), \tag{15}$$

$$SE_R = 10 \log \left(\frac{1}{1-R} \right) = 10 \log \left(\frac{1}{1-|S_{11}|^2} \right), \quad (16)$$

$$SE_A = 10 \log \left(\frac{1-R}{T} \right) = 10 \log \left(\frac{1-|S_{11}|^2}{|S_{12}|^2} \right). \quad (17)$$

3 | NANOCELLULOSE-ASSISTED PREPARATION OF COMPOSITE FILMS

The development of advanced electronic technology has put forward more stringent requirements for EMI films. Light-weight, flexible, robust, corrosion-resistant, and other multifunctional characteristics are highly desired in contrast to the heavy and thick traditional EMI shields. However, new and promising functional nanomaterials such as graphene, MXene, CNTs, and metal nanoparticles are limited in their materials processing by weak interfacial interactions, resulting in an unsatisfactory mechanical property. Thus, the strategy of combining these conductive nanomaterials with nanocellulose in an effort to overcome the structural and mechanical shortcomings has naturally attracted attention. In view of EMI shielding performance, the strong interactions between nanocellulose and functional conductive nanofillers can lead to a tight integration with each other. The electronegativity differences can facilitate the interfacial polarization to promote the attenuation of EMWs, which will be beneficial for enhancing the EMI shielding performance. Using bottom-up fabrication, specific processing routes can have a significant impact on the macrostructures, and a rational structural design can endow materials with enhanced performances and even novel functionalities. Particularly, emulating some of the structures found in natural materials to achieve a specific function is of great potential. In this section, we focus on the assembly pathways and corresponding microstructures of nanocellulose-based EMI shielding films.

3.1 | EMI shielding films with a double-layer coating structure

The EMI shielding films with double-layer coating structures have the characteristics of easy manufacturing, low cost, and simple equipment. Generally, the robust CNF layer acting as the substrate is applied to enhance the mechanical properties, while the surface coatings containing high-conductivity substances take the role of EMI shielding. For example, Parit et al.[132] synthesized polypyrrole (PPy) and CNF-based conducting composite film through the in situ polymerization of pyrrole onto polyvinyl alcohol-coated CNF paper (PPy/PVA-CNP). The composite films delivered an EMI SE of 23 dB with a thickness of 138.4 μm. Meanwhile, the tensile strength reached 103.8 ± 5.9 MPa (with a fracture strain of 11.9% ± 1.7%). Even being completely saturated by water, the film still maintained a tensile strength of 27.4 ± 2.2 MPa (with the fracture strain of 9.4% ± 1.1%). In another example, Cui et al.[133] fabricated $Ti_3C_2T_x$ MXene/CNF composite film via a facile vacuum-assisted filtration method, and the CNF layer was prepared by the electrospinning of cellulose acetate. The composite film exhibited an electrical conductivity of 46,300 S/m, and an EMI SE of 42.7 dB (with 15 μm of $Ti_3C_2T_x$ coating). A promoted tensile strength was observed, as well as a maintained structural integrity after being bent for 500 cycles.

Although the composite films with double-layer coating structures are easy to design and implement, some inherent defects are hard to overcome. For instance, the weak interlayer interaction leads to potential delamination of coatings, and the exposed conductive substances are easily oxidized and eroded, which will result in a dramatic decrease in the EMI shielding performance. To address these issues, Zhou et al.[119] fabricated silicone-encapsulated $Ti_3C_2T_x$/CNF composite films via spray coating. Here, the dispersion containing CNF (derived from paperboards) and $Ti_3C_2T_x$ MXene acting as the ink was repeatedly sprayed on the surface of bacterial cellulose film, and subsequently encapsulated with silicone to improve the hydrophobicity of the resultant composite films (Si-TM/BC) (Figure 2A). Good mechanical properties were also obtained, delivering a high tensile strength (>250 MPa), and desirable toughness (>20 MJ/cm³) (Figure 2B,C). With the coating thickness of only 2.29 μm, the composite film exhibited a superb EMI SE of 30 dB (Figure 2E), as well as the SSE/t of 53,003 dB·cm²/g. When the coating thickness increased to 7.71 μm, the EMI SE reached 60 dB, showing a high EMI shielding ability. The protection from silicone encapsulation was significant, for example, after five times the typical soak-rinse hydration process, the Si-TM/BC films still maintained an EMI SE larger than 20 dB (Figure 2F). Besides the EMI shielding properties, the film also exhibited desirable low voltage-driven Joule heating and photo-responsive heating performances highlighting additional fascinating multifunctionalities, thus broadening the scope of this material.

3.2 | EMI shielding films with alternating-layer structure

Some researchers believed that the coating structure to ensure the high purity of conducting layers is quite important because it avoids the potentially segregating effect of polymer nanofillers that may restrain the highly
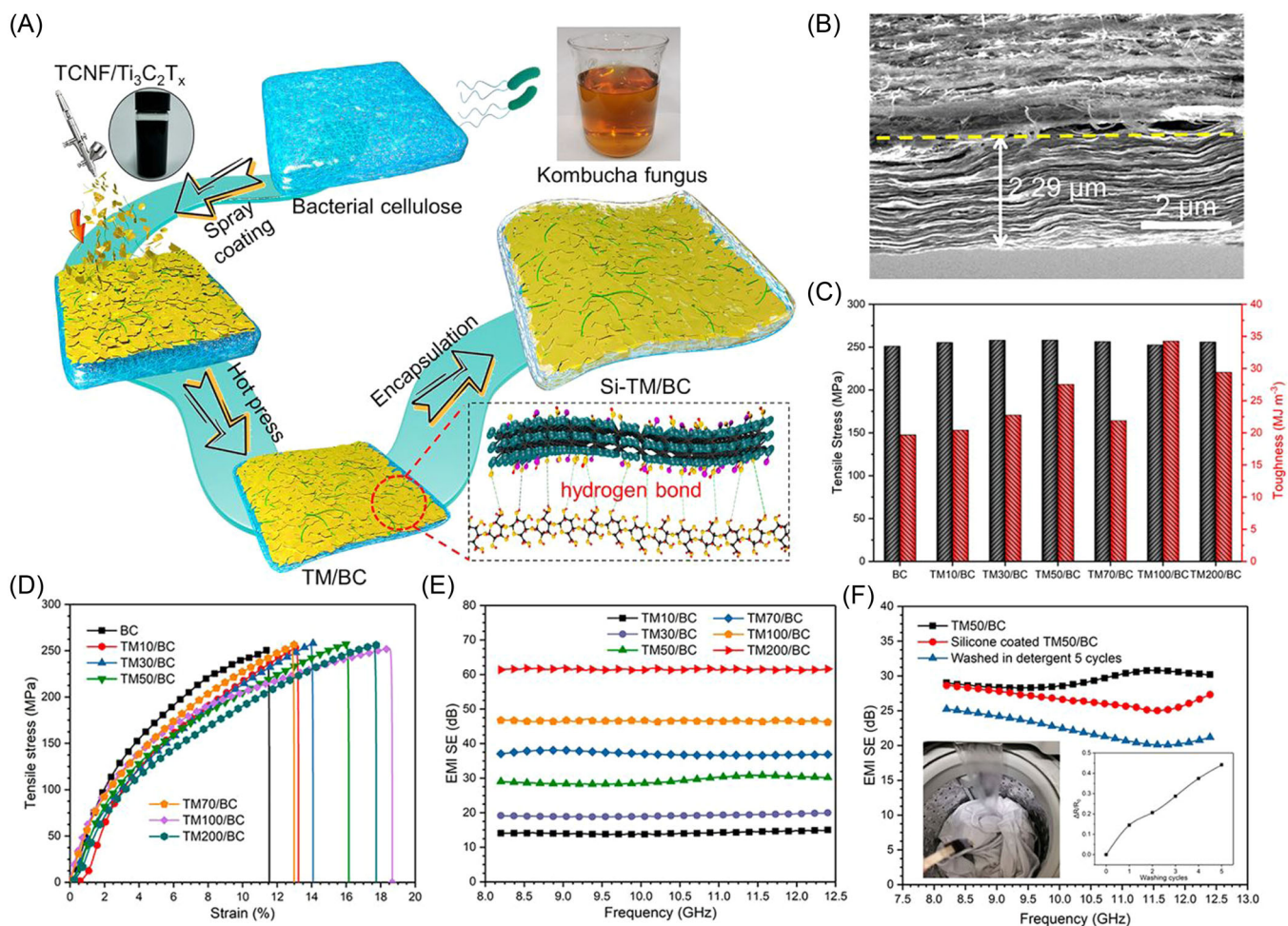
FIGURE 2 (A) Fabrication strategy and appearance of Si-TM/BC film. (B) Scanning electron microscopy cross-section images of TM/BC film. (C) Stress–strain curves of pristine BC and various TM/BC films. (D) Mechanical properties of pristine BC and various TM/BC films. (E) Electromagnetic interference (EMI) shielding effectiveness (SE) of various TM/BC films. (F) The effect of encapsulation on the waterproof stability of EMI SE. Reproduced with permission: Copyright 2021, American Chemical Society.[119]

efficient transferring of electrons in the inhomogeneous layered films. Therefore, inspired by the sedimentary rock formation, ordered deposition of conductive and reinforcing fillers to construct multilayered film with alternating stacked structures can be a potential option to overcome the shortages of the single-layer coating structure. For the nanocellulose-based EMI shielding films with alternating-layer structure, the high-conductivity layers constituted by MXene, reduced graphene oxide (rGO), or CNTs play the role of EMI shielding functions, while the CNF layers are utilized to enhance the mechanical properties of the composite and prevent the crack growth to hold the whole structure without breaking. Meanwhile, the alternating conductive layer can induce multiple reflections inside the films to enhance the shielding performance. For instance, Li et al.[134] fabricated alternating multilayered CNF/graphene nanosheets (GNs) films by using a vacuum filtration process (Figure 3A). The films exhibited an

electrical conductivity of 738 S/m and an SE of 27.4 dB with a thickness of 35 μm. The heterogeneous conductive layers could induce a multiple impedance mismatch to promote the wave reflection. Besides, the films possessed a thermal conductivity of 33.55 W/(m·K) as well. Zhou et al.[135] also assembled CNFs/$Ti_3C_2T_x$ alternating-layer films by repeated vacuum filtration. In the cross-sectional scanning electron microscopy (SEM) images, the alternating multilayered structure was clearly observed (Figure 3B). The film revealed an improved mechanical strength of 112.5 MPa and a toughness of 2.7 MJ/m^3 compared with both freestanding $Ti_3C_2T_x$ and homogeneous CNF/$Ti_3C_2T_x$ films (Figure 3C,D). By studying the tensile fracture surface, the authors noticed that the film had a hierarchical zigzag crack morphology (Figure 3E), and pointed out that the robust CNF layers could prevent the nanosized crack at the $Ti_3C_2T_x$ layer from growing through the whole film (Figure 3F). Meanwhile, the
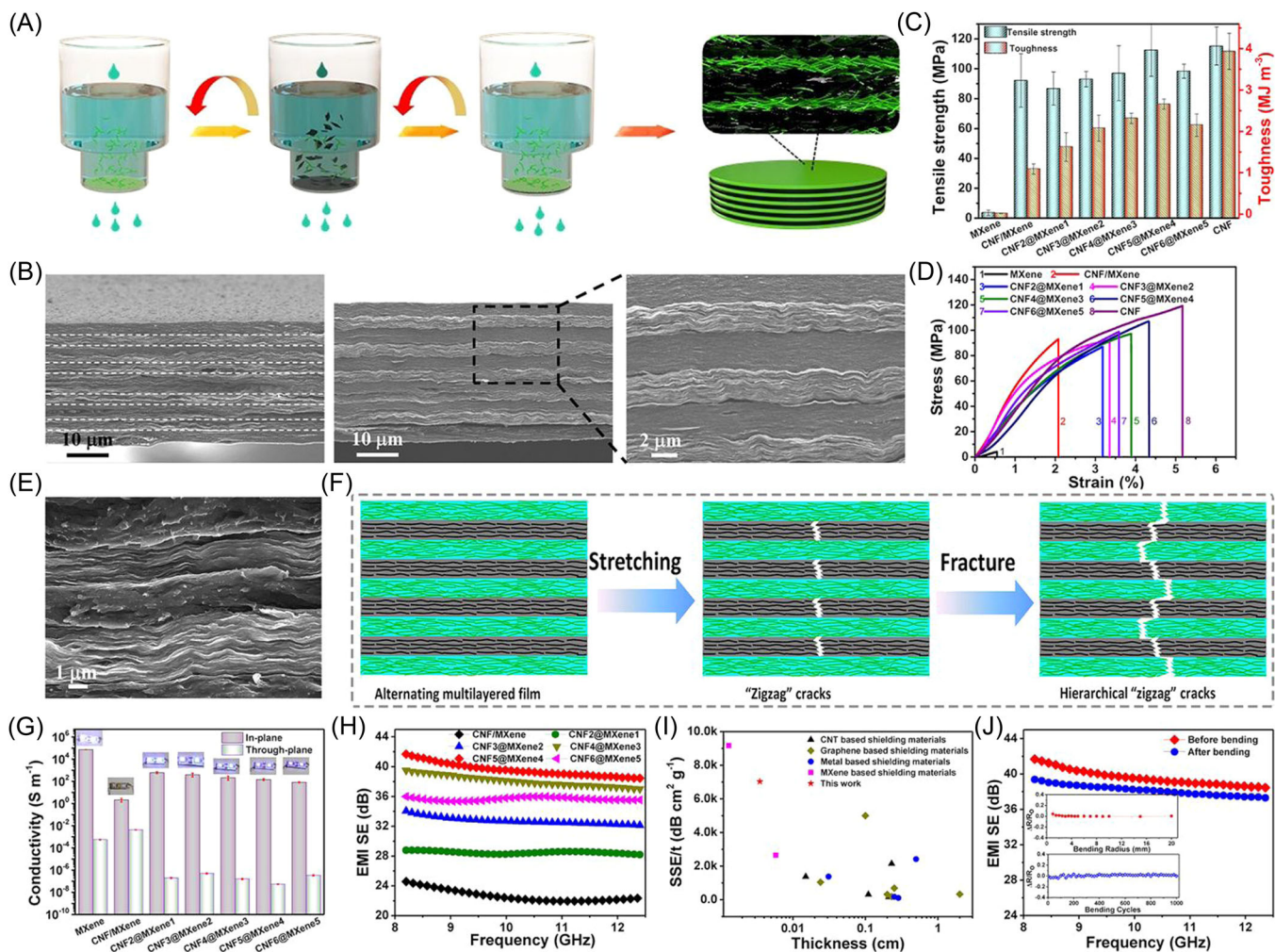
FIGURE 3   (A) Alternating vacuum filtration process to prepare alternating multilayered films. Reproduced with permission: Copyright 2020, Elsevier.[134] (B) Cross-sectional scanning electron microscopy (SEM) images of cellulose nanofibrils/nanofibers (CNFs)/Ti$_3$C$_2$T$_x$ composite films. (C) Tensile strengths, toughness, and (D) tensile stress–strain curves of different CNFs/Ti$_3$C$_2$T$_x$ composite films. (E) SEM micrographs of the fracture surfaces. (F) Schematic illustrations of the fracture mechanism of the alternating multilayered films. (G) Electrical conductivity. (H) Electromagnetic interference (EMI) shielding performance of different CNFs/Ti$_3$C$_2$T$_x$ composite films. (I) EMI shielding performance before and after bending to a radius of 2.0 mm for 1000 cycles. (J) Comparison of specific shielding effectiveness as a function of thickness with other reports. Reproduced with permission: Copyright 2020, American Chemical Society.[135]

film processed the electrical conductivity of 82–621 S/m (Figure 3G), the maximum SE of 40 dB with a thickness of 30–40 μm (Figure 3H), as well the SSE/t of 7029 dB·cm^2/g (Figure 3I). Besides, the composite film still maintained a high electrical conductivity and SE after repeating bending (Figure 3J). Li et al.[117] prepared flexible and tough nanofibrillated cellulose/Fe$_3$O$_4$ and CNT/polyethylene oxide (CNF/Fe$_3$O$_4$&CNT/PEO) films by the alternating vacuum-assisted filtration method. The composite films possessed the tensile strength of 36.03 MPa, toughness of 2.98 MJ/m^3, and elongation at a break of 19.1%. Meanwhile, the EMI SE reached 30.3 dB, with the corresponding electrical conductivity of 3900 S/m. Cao et al.[6] fabricated CNT/CNF/Ti$_3$C$_2$T$_x$ composite papers by alternatingly filtrating the CNT/CNF dispersion and

Ti$_3$C$_2$T$_x$ dispersion. The papers exhibited a tensile strength of 97.9 ± 5.0 MPa, fracture strain of 4.6% ± 0.2%, electrical conductivity of 2506.6 S/m, and EMI SE of 38.4 dB. Although the exploration of EMI shielding films with alternating layered structures was comparatively few, this design strategy still showed a high application prospect.

3.3 | EMI shielding films with "brick-and-mortar" structure

So far, films with "brick-and-mortar" structures are the most attractive and widely studied for the nanocellulose-assisted construction of EMI shielding

films. Inspired by the natural nacre structure, which constituted highly ordered two-dimensional (2D) nano-flaked aragonite and one-dimensional (1D) nanofibrous chitin and protein, some researchers have modeled and constructed nanocellulose-based EMI shielding films with the "brick-and-mortar" structures (Figure 4A). The conductive filler acts as the "brick" to ensure the conductive function, while the nanocellulose plays the part of "mortar" to enhance the interfacial interaction. Thus, the nanocomposite films usually possessed excellent mechanical flexibility and strength. The tight integration brings strong interface interactions that can promote the interfacial polarization attenuation of EMWs, which is in favor of the shielding performance.

Although MXenes have emerged as one of the most promising 2D electrically conductive materials for the construction of EMI shielding films, the weak interfacial interactions between the layers restrain the promotion of mechanical properties and structures. Thus, the introduction of cellulose seems to be a matter of course. Cao et al.[129] prepared ultrathin and highly flexible $Ti_3C_2T_x$/CNF (extracted from garlic husk) nanocomposite papers via a vacuum-filtration-induced self-assembly process. With the 80 wt% $Ti_3C_2T_x$ content, the nanocomposite paper exhibited an undulating layered structure (Figure 4B), and the oriented alignment of $Ti_3C_2T_x$ nanosheets was surrounded by the CNFs. The as-prepared $Ti_3C_2T_x$/CNF composite paper (80 wt% of $Ti_3C_2T_x$) possessed the electrical conductivity of 115.5 S/m
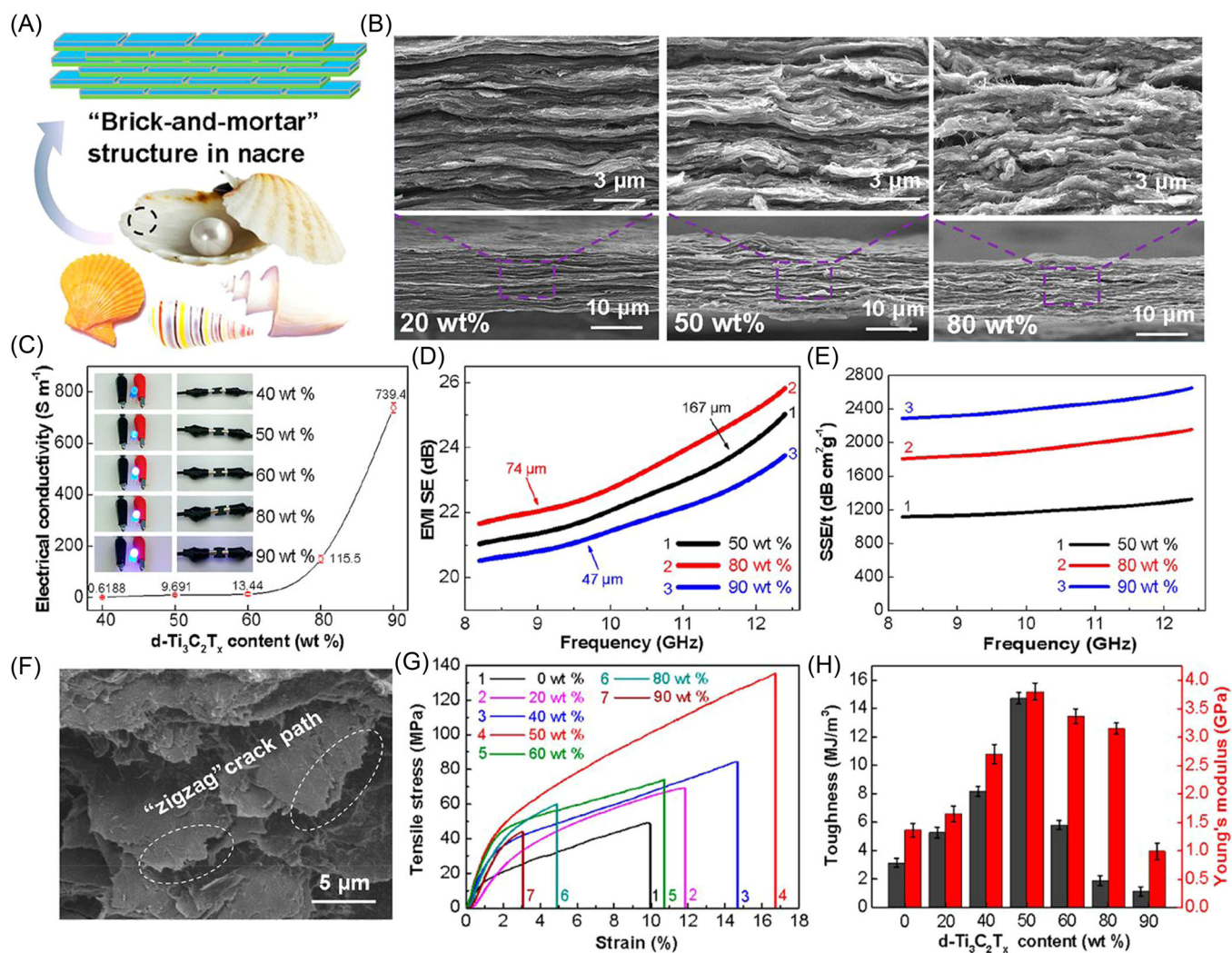
FIGURE 4 (A) Schematic illustration of the "brick-and-mortar" structure in nacre. (B) Scanning electron microscopy (SEM) images, (C) electrical conductivity, (D) electromagnetic interference shielding effectiveness (SE), and (E) Specific SE (SSE)/t of the $Ti_3C_2T_x$/cellulose nanofibrils/nanofiber (CNF) composite paper with various $Ti_3C_2T_x$ contents. (F) SEM image of the fracture surface of the $Ti_3C_2T_x$/CNF composite paper. (G) Tensile stress–strain curves and (H) toughness and Young's modulus of the $Ti_3C_2T_x$/CNF composite paper with various $Ti_3C_2T_x$ contents. Reproduced with permission: Copyright 2018, American Chemical Society.[129]

(Figure 4C), an EMI shielding performance of ~25.8 dB at 12.4 GHz, with a low thickness of 74 μm (Figure 4D), and the maximum SSE/t could reach 2647 dB·cm^2/g (Figure 4E). Meanwhile, the mechanical properties were systematically studied as well. In the case of 50 wt% MXene/CNF composites, the maximum values of the tensile strength (135.4 ± 6.9 MPa), tensile fracture strain (16.7% ± 0.7%), toughness (14.8 ± 0.4 MJ/m^3), and Young's modulus (3.8 ± 0.3 GPa) are shown, and the folding number reached 14,260 times, indicating superb mechanical properties (Figure 4G,H). The authors noticed that the nanocomposite papers exhibited a superior mechanical property compared to both pure MXene papers and pure CNF papers, and a "zigzag" crack path was found on the rough fracture surface (Figure 4F). By investigating the fracture mechanisms, the authors proposed that the hydrogen bonds, flexible CNFs, and anisotropic interconnection networks were the main factors to prevent the fracture of the nanocomposite papers. This study verified the rationality to construct "brick-and-mortar" structures by utilizing CNFs as the bridging material. Similarly, Zhan et al.[136] applied bleached cardboard to extract CNFs and constructed $Ti_3C_2T_x$/TOCNF nanocomposite films by vacuum-assisted filtration. A high electrical conductivity of 2837 S/m and an outstanding EMI shielding ability of 39.6 dB (at the thickness of 38 μm) was achieved. Meanwhile, the $Ti_3C_2T_x$/TOCNF nanocomposite film exhibited a tensile strength of 212 MPa and a Young's modulus of ~7 GPa. Xu et al.[137] prepared $Ti_3C_2T_x$/bacterial (*Acetobacter xylinum*) TOCNF nanocomposite film by the vacuum-assisted filtration as well. Comprehensively considering the mechanical and EMI shielding properties, the composite film with 50 wt% CNF exhibited high tensile strength (252.2 MPa), excellent folding endurance (10,000 times), high electrical conductivity (44,350 S/m), and striking SSE/t (19,652 dB·cm^2/g). Cui et al.[138] freeze-dried the film $Ti_3C_2T_x$/CNF precursor (assembled by vacuum filtration) to maintain a certain degree of pore structure leading to a density of the obtained composite film that declined (1.3 ± 0.1 g/cm). Meanwhile, under the 10 wt% CNFs additive content, the EMI SE reached 50 dB and the SSE/t was 9177 dB·cm^2/g. Besides, Liu et al.[139] filtrated a mixture of silver nanowires (AgNWs), CNFs, and $Ti_3C_2T_x$. The fabricated $Ti_3C_2T_x$/AgNWs/CNFs composite films possessed the tensile strength of 100.3 MPa, EMI SE of 46.6 dB with a thickness of 9.5 μm, and SSE/t of 19,613.5 dB·cm^2/g.

The same preparation strategy can be referred to for the construction of graphene/CNF composite films. For example, Yang et al.[140] filtrated the rGO/CNF composite film by vacuum-assisted filtration and subsequent reduction treatment. The composite film (50 wt% CNF loadings) exhibited the remarkable electrical conductivity of 4057.3 S/m and EMI SE of 26.2 dB. The mechanical properties of the rGO/CNF composite film were enhanced with the raising CNF contents as well. The composite film possessed a tensile strength of 67.7 ± 2.9 MPa, Young's modulus of 7737.9 ± 77.5 GPa, and fracture elongation of 1.4% ± 0.2%. To achieve a green preparation approach, Wiemann et al.[141] applied the GNs to replace the rGO (aiming to avoid the unfriendly reduction treatment). The GN/TOCNF composite films were assembled by vacuum-assisted filtration and subsequent mechanical compression. The composite film (10 wt% CNF loadings) delivered the tensile strength of 61 MPa, Young's modulus of 4.7 GPa, and fracture elongation of 2.1%. Meanwhile, an electrical conductivity of 98,820 S/m was achieved, accompanied by an EMI SE of 43 dB with only 13 μm thickness. To introduce extra magnetic loss, Han et al.[73] decorated rGO with metallic Ni nanoparticles (rGO@Ni) via a hydrothermal reaction and then fabricated the CNF/rGO@Ni composite film through the vacuum-assisted filtration. The films exhibited an electrical conductivity of 262.7 S/m and an EMI SE of 32 dB (~15–20 μm).

Moreover, some researchers utilized the CNFs to assist to exfoliate the expandable graphite (EG). Zhang et al.[142] prepared the CNFs/few-layer graphene dispersions via the wet comilling method and fabricated the composite films by vacuum filtration and hot pressing. The films possessed a tensile strength of 59.14 MPa, Young's modulus of 4.13 GPa, and fracture elongation of 4.17%, as well as a marginal EMI SE of 10 dB. Yuan et al.[64] prepared the zeolitic imidazolate framework-67 (ZIF-67)-derived porous carbon (C-ZIF67)/graphene nanoplate/CNF composite films, which exhibited a tensile strength of 46.33 MPa and an EMI SE value of 50.5 dB. Yang et al.[143] fabricated the EG/CNF/PEO composite film by sonicating the EG/CNF dispersion, filtrating the mixture with extra PEO addition, and final mechanical pressing. The composite film displayed a tensile strength of 63.3 MPa, electrical conductivity of 122,600 S/m, and EMI SE of 44 dB (12 μm). This strategy to produce EMI shielding films is regarded as flexible, environmentally friendly, and cost-effective, in accordance with the expectation of "green" chemical technology.

In particular, the abovementioned "brick-and-mortar"-structure films are restricted to physical cross-linking, and the mechanical enhancement largely depends on the hydrogen bonds between the "bricks" and "mortars." To get further performance improvements, Wu et al.[118] proposed the physical and chemical dual cross-linking method to fabricate CNFs/$Ti_3C_2T_x$ nanocomposite films (PC-MXene). The miscible liquids containing CNFs (extracted from bleached softwood pulp fibers) and $Ti_3C_2T_x$ were dried in a polypropylene mold under

ambient pressure and were then immersed in an acetonitrile/methyl caproate solution with a 10% poly ((phenyl isocyanate)-*co*-formaldehyde) (PMDI) to achieve chemical cross-linking (Figure 5A). As expected, the extra strong covalent interactions (urethane bonding) led to robust and freestanding films with a thickness as low as 0.9 μm, and the introduction of a hydrophobic PMDI backbone endowed the PC-MXene films with superb stability and water resistance. Meanwhile, the PC-MXene films showed a significant enhancement in tensile strength, Young's modulus, and mechanical toughness compared to the CNFs/Ti$_3$C$_2$T$_x$ films without chemical crosslinking (Figure 5C,D). The high electrical conductivity (211 and 300 S/m; Figure 5E) ensured the excellent EMI shielding performance. With the thicknesses of 0.9–15 μm, the EMI SE reached 33.3–73.8 dB, and the addition of CNFs did not cause significant shielding performance loss (Figure 5F,G). The PC-MXene film also delivered an extraordinary SSE/t value of 148,000 dB·cm^2/g, which surpassed most films ever
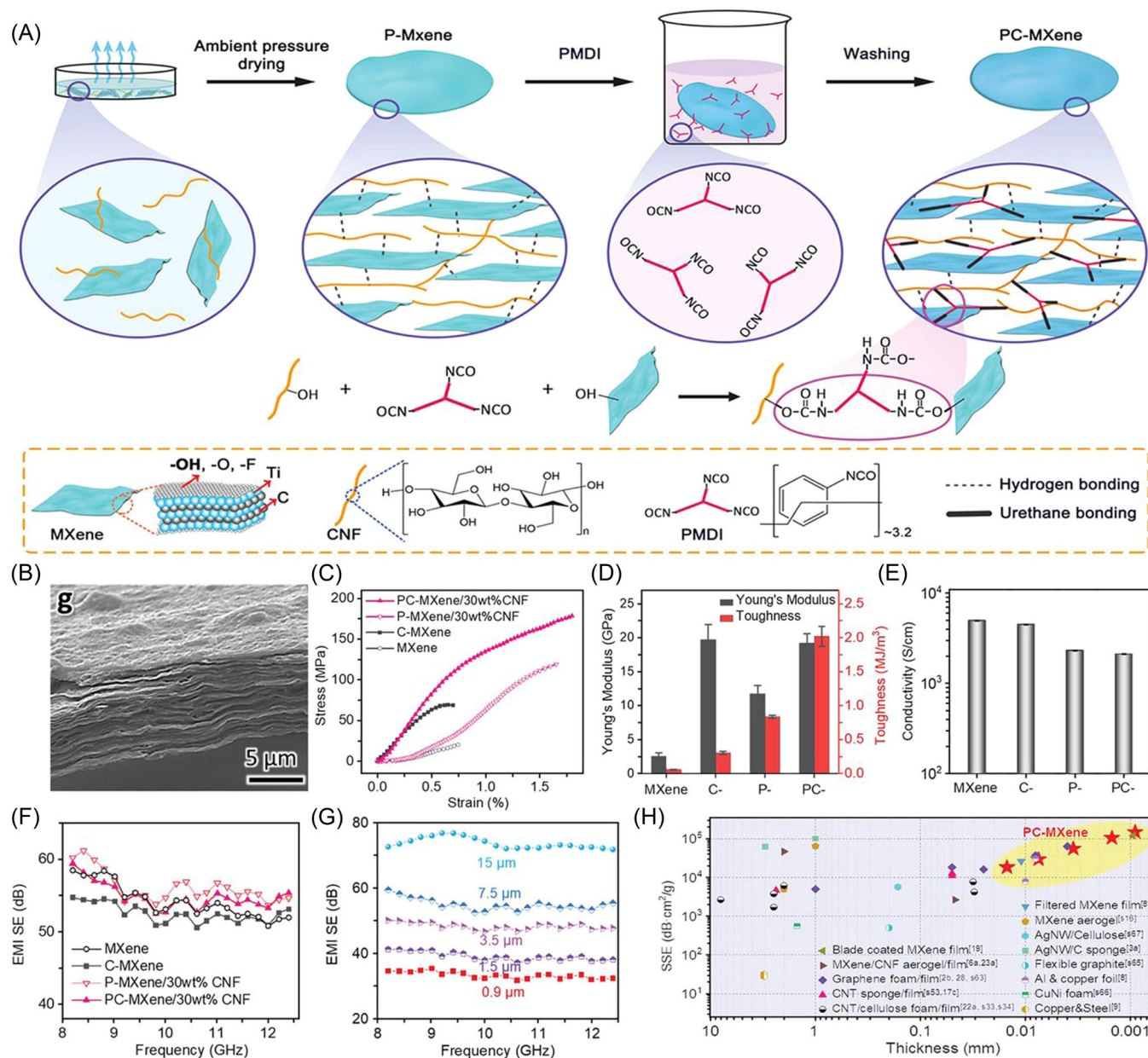
FIGURE 5 (A) Schematic of the physical and chemical dual cross-linking preparation process for PC-metal carbides/nitride (MXene). (B) Scanning electron microscopy (SEM) images of the PC-MXene film, (C) tensile stress–strain curves and (D) corresponding modulus and toughness, (E) electrical conductivity, and (F) electromagnetic interference (EMI) SE of MXene, chemical cross-linking Ti$_3$C$_2$T$_x$ (C-MXene), physical cross-linking cellulose nanofibrils (CNFs)/Ti$_3$C$_2$T$_x$ (P-MXene), and PC-MXene film. (G) EMI SE and (H) specific SE of PC-MXene film. Reproduced with permission: Copyright 2021, Wiley.[118]

reported (Figure 5H). The authors affirmed the positive role of the nacre-like "brick-and-mortar" structure in the excellent performance, which truly facilitated the synergy between $Ti_3C_2T_x$ and CNFs. This study provided a conspicuous strategy to fabricate high-performance EMI shielding films and is potentially of great significance for the development of next-generation electronic devices.

3.4 | EMI shielding films with other structures

Some CNF-based composite films with other structures have also been investigated for efficient EMI shielding. Derived from the "brick-and-mortar" structure, some research replaced the 2D electrical conductivity substance with the 1D nanomaterials such as CNTs and metallic AgNWs to construct a long-range conductive network. For example, Lapka et al.[144] assembled PPy nanotubes (PPy-NTs)/CNF, carbonized C-PPy-NTs)/CNF, and multiwalled CNTs (MWCNTs)/CNF composite films by drying the mixed dispersion in a specific mold and investigated their EMI shielding performance. The PPy-NT/CNF film exhibited a more efficient EMI SE (~12 dB, 140 μm) than the MWCNTs/CNF (~9 dB) and C-PPy-NT/CNF (<1 dB) films. Zhang et al.[145] fabricated MWCNT/CNF (extracted from bleached softwood pulp) composite films via vacuum-assisted filtration and subsequent hot-pressing. This composite film (thickness 0.15 mm) showed an EMI SE of 45.8 dB, as well a corresponding SSE/t of 3563.6 dB·cm²/g. Due to the all-fiber structure, the composite film possessed good flexibility and tensile strength up to 48 MPa. Chen et al.[58] fabricated CNF/AgNW composite papers through vacuum-assisted filtration. With a 40-μm thickness, the paper possessed a high electrical conductivity (102,190 S/m) and EMI SE (39.3 dB). Meanwhile, the excellent tensile strength (49.1 MPa) and high flexibility and durability (>2000 bending) endowed the papers with satisfactory mechanical properties.

Utilizing conductive macromolecules as the fillers, in situ polymerization to form a fiber-coated structure is also a considerable way. For instance, Gopakumar et al.[146] prepared bending-resistance polyaniline (PANI)/CNF composite films via the in situ polymerization of aniline on CNFs, and the PANI was continuously coated on the CNFs. The composite film exhibited an electrical conductivity of 31.4 S/m, and an average EMI SE of 23 dB with a thickness of 1 mm. Zhang et al.[147] prepared a PANI/CNF (extracted from poplar wood fibers) membrane with core–shell heterostructure by in situ polymerization. The membrane delivered an electrical conductivity of 227 S/m, as well the EMI SE of 25.2 dB with a thickness of 0.28 mm.

In addition, some composite films with unique structures such as graphene/bacterial cellulose papers (graphene nanosheets are bundled by bacterial cellulose)[148] and CNF/MWCNT/$Ti_3C_2T_x$ films (yarn-ball-shaped CNF/MWCNT microspheres are intercalated in $Ti_3C_2T_x$ inter-lamination)[149] were prepared. Considering that these studies are sporadic and of special interest, they are not discussed systematically here. To easily compare the discrepancies leading from different strategies, the mechanical and EMI properties of nanocellulose-based composite films were listed in Table 1.[149–154]

4 | NANOCELLULOSE-ASSISTED PREPARATION OF COMPOSITE AEROGELS

The integration of porous microstructure is becoming more desirable for preparing high-performance EMI shielding architectures with low density and high strength-to-weight ratio. Moreover, the introduced porous structure is beneficial for improving the multiple reflections of incident EMWs and thus increasing the interactions between the EMWs and cell walls. Combined with an efficient EMW loss capability of the cell walls, the EMI shielding performance of the porous architectures can be enhanced.[79,155–161] Herein, rational design and controlled assembly of the porous EMI shields based on various functional nanomaterials are crucial. At this point, the nanocellulose, especially the CNF, with excellent mechanical properties, high aspect ratio, large specific surface area, and diverse surface chemistry is promising, as it can have strong interactions with functional nanomaterials, such as metal nanoparticles, CNT, graphene, and MXene layers. This leads to the efficient assembly or construction of high-performance EMI shielding aerogels with good mechanical strength, low density, and high EMI shielding performance. In this section, some representative nanocellulose-based EMI shielding porous structures are summarized with the focus on advancing the understanding of relationships between the structure and functionalities.

4.1 | EMI shielding aerogels with random pore structures

Compared with the porous EMI shields composed of cellulose as a matrix and embedded with various functional nanomaterials, the CNFs have a higher potential for preparing composite aerogels with high mechanical strength.[162–164] This can be ascribed to the stronger interfaces between the functional nanomaterials and nanocellulose. In addition, efficient conductive paths

TABLE 1 The mechanical and EMI properties of nanocellulose-based composite films.

Structure	Material	Mechanical property			EMI property				Ref.
		Tensile strength (MPa)	Fracture strain (%)	Toughness (MJ/m³)	SE (dB)	Thickness (μm)	SSE/t (dB·cm²/g)	Electrical conductivity (S/m)	
Double-layer coating structure	PPy/PVA-CNP	103.8	11.9	/	23	138.4	/	6	[132]
	$Ti_3C_2T_x$/CNF	/	68	/	42.7	15	/	46,300	[133]
	Si-$Ti_3C_2T_x$/CNF	>250	>11.5	>20	30	2.29	53,003	/	[119]
Alternating-layer structure	CNF/graphene	/	/	/	27.4	35	/	738	[134]
	CNF/$Ti_3C_2T_x$	112.5	4.3	2.7	40	30–40	7029	621	[135]
	CNF/Fe_3O_4&CNT/PEO	36.03	19.1	2.98	30.3	24.95	/	3900	[117]
	CNT/CNF/$Ti_3C_2T_x$	97.9	4.6	2.1	38.4	38	8020	2506.6	[6]
"Brick-and-mortar" structure	$Ti_3C_2T_x$/CNF	135.4	16.7	14.8	25.8	74	2647	115.5	[129]
	$Ti_3C_2T_x$/TOCNF	212	4.3	5.5	39.6	38	4750	2837	[136]
	$Ti_3C_2T_x$/A-CNF	252.2	2.6	3.2	41.2	11.4	19,652	44,350	[137]
	$Ti_3C_2T_x$/CNF	65	1.4	/	50	/	9177	24,875	[138]
	$Ti_3C_2T_x$/AgNW/CNF	100.3	0.84	0.42	46.6	9.5	19,613.5	163,200	[139]
	rGO/CNF	67.7	1.4	/	26.2	23	/	4057.3	[140]
	Graphene/CNF	61	2.1	/	43	13	/	98,820	[141]
	CNF/rGO@Ni	/	/	/	32	15–20	/	262.7	[73]
	CNF/FLG	59.14	4.17	/	10	/	/	18	[142]
	C-ZIF67/GNP/CNF	46.33	>13.5	/	50.5	100	/	6173	[64]
	EG/CNF/PEO	63.3	1.1	/	44	12	/	122,600	[143]
	CNC/RGO	227	4.1	5.17	39.1	12	11,367	2445	[150]
	CNF/PC-$Ti_3C_2T_x$	>175	>1.25	2.0	73.8	15	148,000	211,300	[118]
	CNF/$Ti_3C_2T_x$/h-BN	11.14	~0.52	/	37.29	47.6	8648.26	5767	[151]
	CNF/$Ti_3C_2T_x$/AgNW	63.8	~1.5	/	42	16.9	16,724	~30,000	[152]
	CNF/$Ti_3C_2T_x$/g-C_3N_4	23.85	0.72	/	42.99	28.2	9331.2	169.5	[153]

TABLE 1 (Continued)

Structure	Material	Mechanical property			EMI property			Electrical conductivity (S/m)	Ref.
		Tensile strength (MPa)	Fracture strain (%)	Toughness (MJ/m^3)	SE (dB)	Thickness (μm)	SSE/t (dB·cm^2/g)		
Other structure	PPy-NT/CNF	/	/	/	~12	140	/	1.16	[144]
	MWCNT/CNF	48	3.5	/	45.8	150	3563.6	3024	[145]
	CNF/AgNW	49.1	4.5	/	39.3	40	/	102,190	[58]
	CNF/AgNW	17.22	2.4	/	93.8	167.2	/	1,000,000	[154]
	PANI/CNF	/	/	/	23	1000	/	31.4	[146]
	PANI/CNF	/	/	/	25.2	280	/	227	[147]
	CNF/MWCNT/Ti$_3$C$_2$T$_x$	7.6	2.3	/	45.1	43.0	/	138	[149]

Abbreviations: AgNW, silver nanowire; CNC, cellulose nanocrystal; CNF, cellulose nanofibrils/nanofiber; CNT, carbon nanotube; FLG, few layer graphene; hBD, hexagonal boron nitride; MWCNT, multiwalled CNT; PANI, polyaniline; PEO, polyethylene oxide; PPy, polypyrrole; PVA, polyvinyl alcohol; rGO, reduced graphene oxide.

derived from the good dispersion of the conductive nanomaterials can be obtained in the nanocellulose-based composites aerogels. Therefore, a high EMI shielding performance of the low-density yet robust nanocellulose-based composite aerogels is promising (Figure 6). For instance, Zhang et al.[162] fabricated the CNF/ammonium polyphosphate (APP)/Ti$_3$C$_2$T$_x$ MXene composite aerogels via freezing the precursor CNF/APP/MXene mixed dispersion in a freezer at −60°C, followed by the freeze-drying process. The CNF with a length of 1–3 μm and diameter of 3–10 nm could first adhere well with the MXene and APP because of the hydrophilic functional groups and formed intact composite cell walls. In other words, the MXene and APP were efficiently dispersed in the nanocellulose-based composite cell walls of the aerogels. The APP furthermore led to an excellent fire resistance of the resultant CNF/APP/MXene composite aerogels without obvious shrinkage upon contact with the flame of an alcohol burner. MXene-based conductive paths were well established in the composite, contributing to the good conductivity (12 S/m) and EMI SE of the aerogels. Moreover, the MXene contents were well controlled, which was instrumental in the EMI SE controllability of the composite aerogel. Furthermore, the porous structure could improve the multiple reflections of incident EMWs, contributing to the interactions between the cell walls and EMWs and thus improving the EMI shielding performance. The composite aerogel containing 60 wt% MXene showed an average EMI SE of 55 dB at a thickness of 8 mm, corresponding to an SSE/t value of ~5729 dB·cm^2/g. Xin et al.[163] employed 1D CNF to assist the construction of three-dimensional (3D) MXene-based frameworks to overcome the weak interlayer bonding force between MXene nanolayers. The composite aerogel had a 3D porous structure, where the internal structure was formed by 1D CNFs and a tightly attached 2D MXene layer. The composite aerogels achieved an electrical conductivity of ~65.6 S/m and an EMI SE of 39.5 dB. Furthermore, the silicone coating on the MXene/CNF aerogel was carried out, resulting in the implementation of hydrophobicity and water resistance, which is vital for maintaining a satisfactory lightweight aerogel in a wet environment. Especially, the silicone-coated MXene/CNF aerogels also exhibited good Joule heating and photothermal performance, showing the promising application potentials of the multifunctional silicone–MXene/CNF aerogels. CNF could further act as a carbon source for preparing carbon-based EMI shielding composite aerogels. An aerogel composed of CNFs stringing polyhedral Co/C particles has been fabricated via in situ growth of ZIF-67 on BC, followed by the pyrolysis under argon.[164] The 3D carbon-based porous structure with interconnected network and the magnetic Co/C particle embedded contributed to the high conduction loss, strong magnetic loss, and multiple polarization loss of
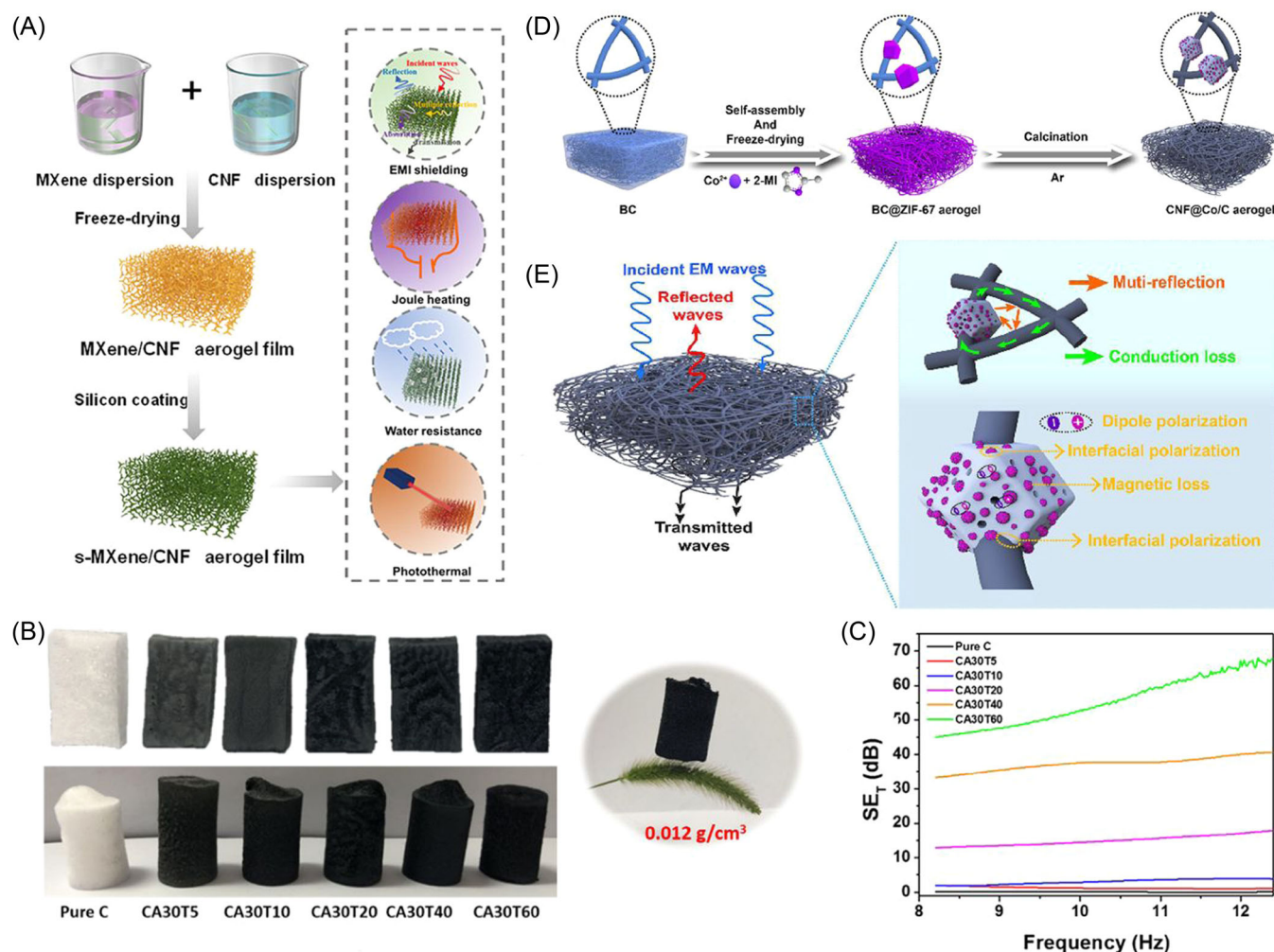
FIGURE 6 (A) Schematic illustrating the preparation process of silicone−metal carbides/nitride (MXene)/cellulose nanofibril (CNF) aerogel films with superior multifunctional performance (electromagnetic interference (EMI) shielding, Joule heating, water resistance, and photothermal performance). Reproduced with permission: Copyright 2021, American Chemical Society.[163] (B) The digital photos of pure cellulose aerogel, CNF/APP/$Ti_3C_2T_x$ hybrid aerogels and CNF/APP/$Ti_3C_2T_x$ hybrid aerogel on a *Setaria viridis*. (C) EMI shielding performance of CNF/APP/$Ti_3C_2T_x$ hybrid aerogels during X-band. Reproduced with permission: Copyright 2021, Elsevier.[162] (D) Schematic illustration of the synthesis of CNF@Co/C aerogels. (E) Possible EMI shielding mechanism of CNF@Co/C aerogel. Reproduced with permission: Copyright 2020, Elsevier.[164]

the composites. The resultant composite aerogels thus exhibited a high X-band EMI SE approaching 56.07 dB at a density of 0.023 g/cm³, and an average absorption coefficient of 0.79.

4.2 | EMI shielding aerogels with aligned pore structures

In addition to adjusting the constituents and contents of composites, controlling the pore morphologies was highly promising for adjusting the EMI shielding performance. The high mechanical properties of nanocellulose provide the potential to construct a stable and orderly pore structure. Compared with the randomly crosslinked pores, the high anisotropy of aligned pores

brings unique functionalities for EMI shielding aerogels. Combined with the high EMW loss capability of the cell walls, the enhanced multiple reflections of incident EMWs upon propagating perpendicular to the aligned pore channels/cell walls can increase the EMI shielding of the aerogels. Meanwhile, the aligned porous structure changes the mechanical properties in different directions. This provides the possibility of fabricating some special shielding devices and attracts more and more attention. In this regard, the extensively confirmed structure-directing function of CNFs derived from the strong tendency of CNF to form intact films promised the construction of composite aerogels with aligned cell walls or pore channels.[78,162,165,166] In our previous work,[70] owing to the highly efficient utilization of the CNFs, various pore morphologies, including lamellar,

honeycomb-like, and random micrometer-sized pores of CNF/AgNW composite aerogels, were successfully achieved via an ice-templated freeze-drying approach (Figure 7). The large-aspect-ratio CNFs were efficiently utilized to stabilize and interact with the as-prepared highly conductive AgNWs. The comparisons of

the composite aerogels with various pore morphologies promoted the understanding between the pore microstructure and macroscopic properties involving mechanical, electrical, and EMI shielding performance. This is vitally important for the design and development of high-performance EMI shielding materials or architectures.
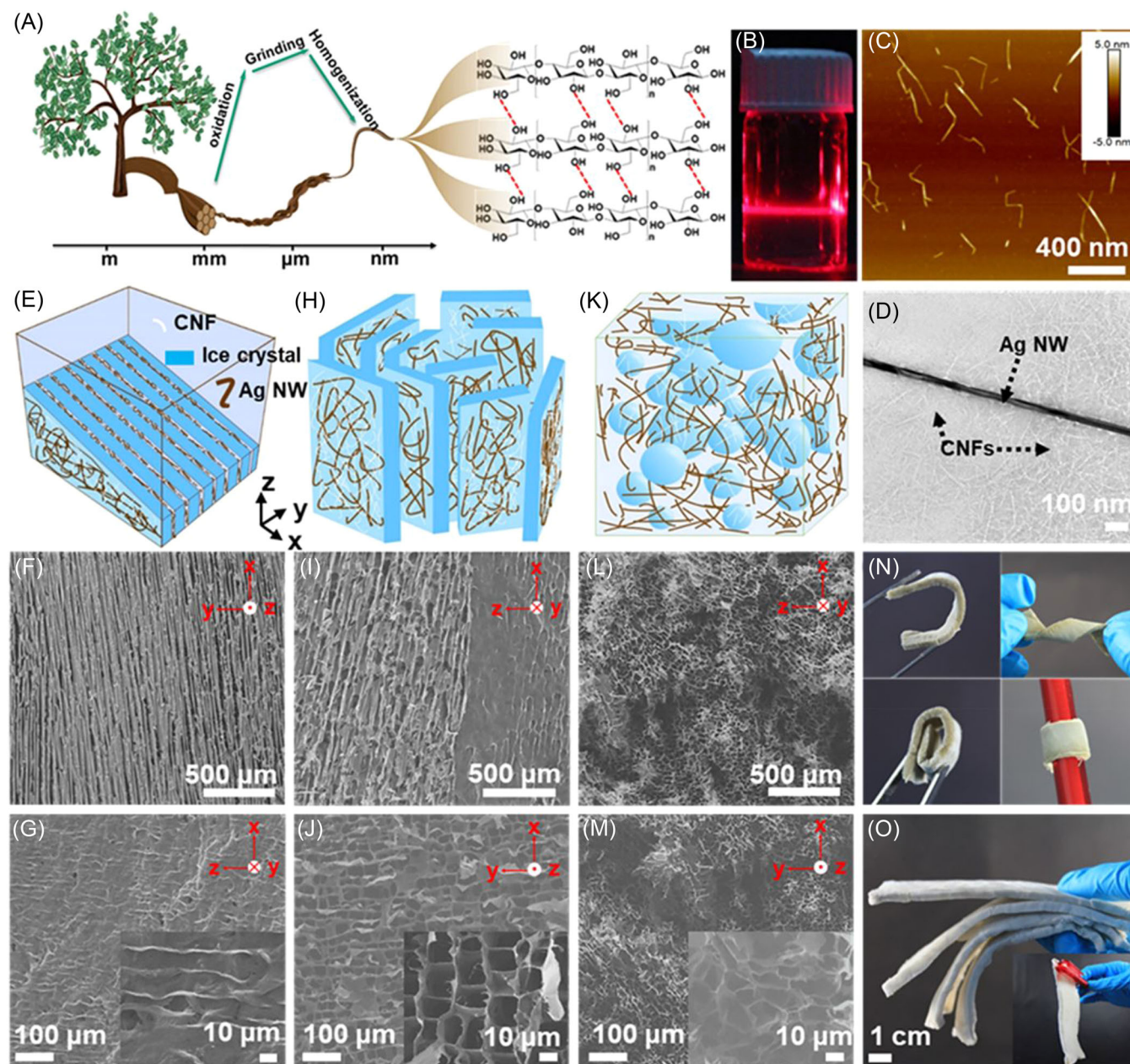

FIGURE 7 (A) Schematic of the cellulose nanofibril (CNF) preparation process, (B) photograph of the CNF dispersion showing the typical Tyndall effect, (C) atomic-force microscopy image of the as-prepared CNFs, and (D) transmission electron microscope (TEM) image showing the good attraction between the CNFs and silver nanowire (AgNW) and adhesion of CNFs on the AgNW. Schematic illustrations of the growth of the ice crystals in various freezing approaches for the CNF/AgNW dispersion and scanning electron microscopy (SEM) images of the corresponding aerogels: (E–G) bidirectional, (H–J) unidirectional, and (K–M) uniform/random freezing. (N) Ultralight and flexible performances (bendability, twistability, and rollability) of the aerogels at a density of 6.2 mg/cm^3. (O) Demonstration of large-area lamellar porous biopolymer aerogels with various densities of (from top to bottom) 10.0, 3.9, 2.0, and 1.7 mg/cm^3 (inset, a large-area aerogel with a density of 2.0 mg/cm^3 held up by the electrostatic force). Reproduced with permission: Copyright 2020, American Chemical Society.[70]

An optimized mass ratio of cellulose to AgNWs, along with synergistic effects of multiple reflections derived from the lamellar cell wall–void interfaces and the absorption and reflection capability arising from composite cell walls, led to the outstanding EMI shielding properties of the composite aerogels. The 2-mm-thick AgNW/CNF composite lamellar porous aerogels achieved an EMI SE of around 70–40 dB in the X-band, while the density was merely 6.2–1.7 mg/cm^3, respectively. The corresponding SSE/t values were up to 178, 235 dB·cm^2/g, significantly outperforming other shielding materials ever reported. Moreover, the composite aerogels also showed good antibacterial performance, further extending the versatility and application fields of these biopolymer aerogels.

More CNF-based composite aerogels with aligned pore morphologies have been prepared for EMI shielding application. Chen et al.[165] reported the fabrication of wood-inspired anisotropic CNF/AgNW composite aerogels with well-aligned and oriented pore channels. Attributed to the synergistic coactions between the CNFs and highly conductive and large-aspect-ratio AgNWs, the composite aerogels showed excellent mechanical strength and structural stability, high EMI shielding, and functionalities including fast thermal diffusion, effective electrothermal heating effect, and high electromechanical sensing performance. Furthermore, Chen et al.[166] embedded the chemical coprecipitated AgNW@Fe$_3$O$_4$ into the CNF-based honeycomb-like composite aerogels. The synergistic coactions of CNFs, AgNWs, Fe$_3$O$_4$, and aligned porous structure led to the low density (16.76 mg/cm^3), good saturation magnetization (4.21 emu/g) and electrical conductivity (0.02 S/cm), and anisotropic EMI shielding ability of the composite aerogels. Li et al.[78] prepared the low-density and compressible CNF/rGO carbon aerogel via the unidirectional freeze-drying and pyrolysis processes. The CNF-based carbon aerogels with unidirectionally aligned pores showed better compression resilience and EMI shielding performance in the direction perpendicular to the pore channels. The aerogel exhibited an X-Band EMI SE of ~33 dB at a low density of 0.0058 g/cm^3, corresponding to a specific EMI SE of 5759 dB·cm^3/g. Wang et al.[167] fabricated the 3D highly electrically conductive CNF/Ti$_3$C$_2$T$_x$ MXene aerogels (CTA) with aligned porous structures via directional freeze-drying, followed by the thermally annealed process. The MXene and CNF supported each other, thus preventing agglomeration of each component, and promoting the formation of an aligned porous structure that would not be altered after annealing. The robust composite aerogels were further infiltrated into

the epoxy to form the nanocomposites via a vacuum-assisted impregnation and curing method. The results showed that the nanocomposites had an ultralow percolation threshold of 0.20 vol% MXene because of the 3D highly conductive networks. When the volume fraction of MXene was 1.38 vol%, the electrical conductivity, EMI SE, and SE divided by thickness (SE/d) values of the nanocomposites reached 1672 S/m, 74 dB, and 37 dB/mm, respectively, which were almost the highest values compared to those of polymer nanocomposites reported previously at the same filler content. In addition, the EMI SE value of the nanocomposites in the radial direction (74 dB) was much higher than that in the axial direction (57 dB), presenting an anisotropic EMI shielding behavior. Fei et al.[168] manufactured a 3D ultralight Co/C@CNF carbon aerogel via directional freeze-casting of CNF anchored ZIF-67, followed by the annealing process (Figure 8). The resultant composite aerogels are composed of aligned pore channels and interconnected carbon sheet networks embedded with Co/C nanoparticles. Remarkably, the composite aerogels displayed a high EMI SE of 35.1 dB at a density of only 1.74 mg/cm^3, corresponding to the highest SSE reaching 20172.4 dB·cm^3/g. This good performance originated from the magnetic Co nanoparticles embedded in the CNF-derived carbon sheet and the porous structure, enhancing magnetic loss and dielectric loss ability.

The investigation of the influences of aligned porous structure on the EMI shielding performance mainly depended on the propagation direction of incident EMWs. However, with respect to the electric field, the EMI shielding performance of the aligned porous aerogels could also be controlled. In our previous work, we employed the CNF to assist in the fabrication of ultralow-density MXene aerogels through a unidirectional freeze-drying approach (Figure 9).[46] The MXene/CNF composite aerogels exhibited apparent aligned honeycomb-like pore morphology. Particularly, the EMI shielding performance was controlled by adjusting the orientation of the cell walls, for example, an angle of 0° was defined when the oriented pore channels were parallel to the electric field direction of incident EMWs, which corresponded to a maximum EMI SE of 63 dB of the aerogels. With increasing angles from 0° to 90°, the EMI SE decreased from 63 to 37 dB. Therefore, a significant influence of the angles between oriented cell walls and the incident EM wave electric field direction on the EMI shielding performance was revealed, showing a vital microstructure design strategy. In addition, MXene "bricks" bonded by the CNF "mortars" of the nacre-like cell walls contributed to the high mechanical strength and flexibility, good electrical conductivity, and ultrahigh EMI
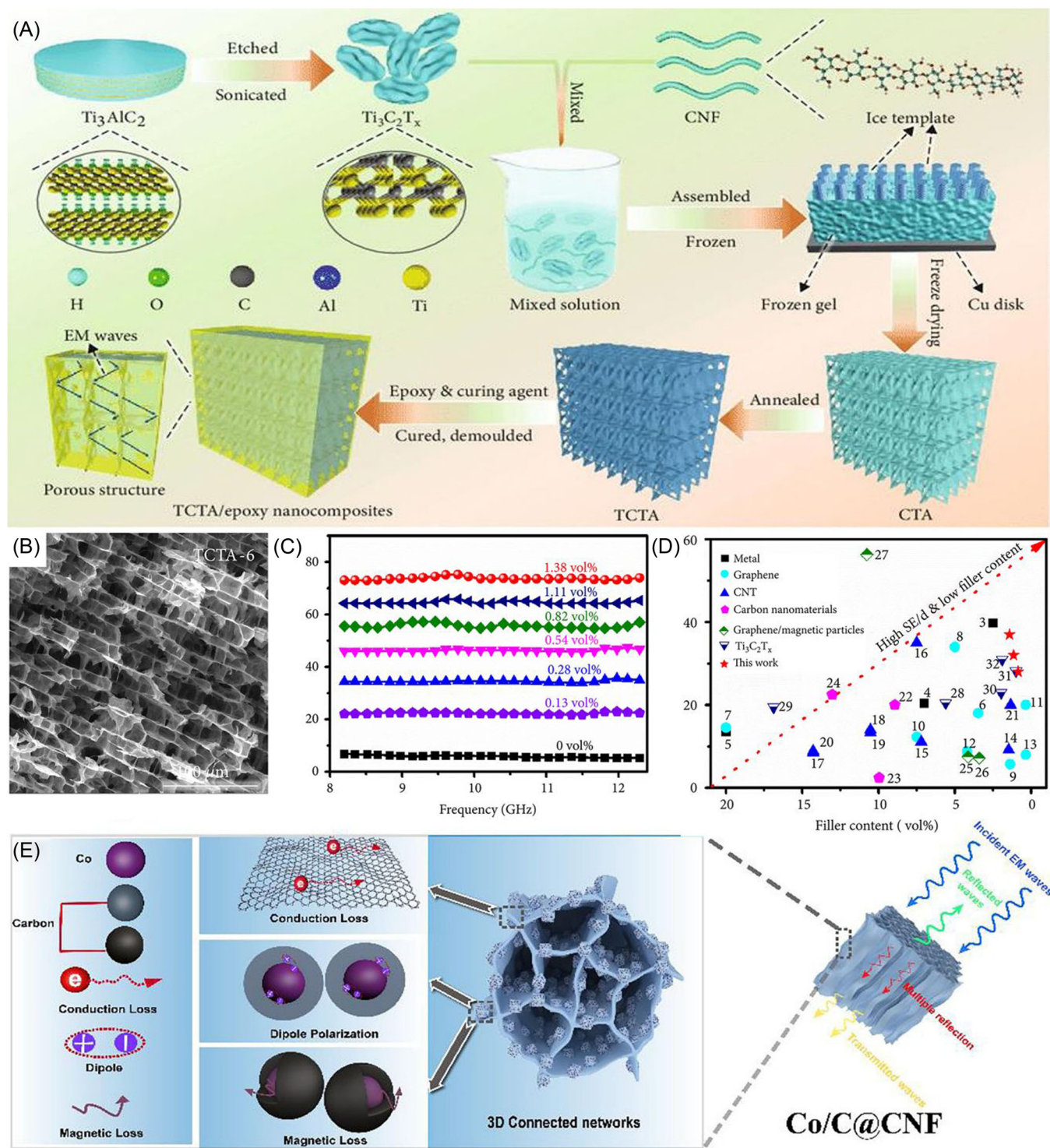
FIGURE 8 (A) Schematic illustration of fabrication for TCTA/epoxy nanocomposites. (B) Scanning electron microscopy (SEM) image of TCTA-6. (C) Electromagnetic interference (EMI) shielding effectiveness (SE) values of the TCTA/epoxy nanocomposites at X-band. (D) Comparison of EMI SE values for TCTA-6/epoxy nanocomposites (marked as red stars) with those of other reported works. SE/d is depicted as a function of conductive filler volume fraction. Reproduced with permission: Copyright 2020, Research.[167] (E) Schematic representation of the EMI shielding mechanism of Co/C@CNF aerogel. Reproduced with permission: Copyright 2021, Elsevier.[168]
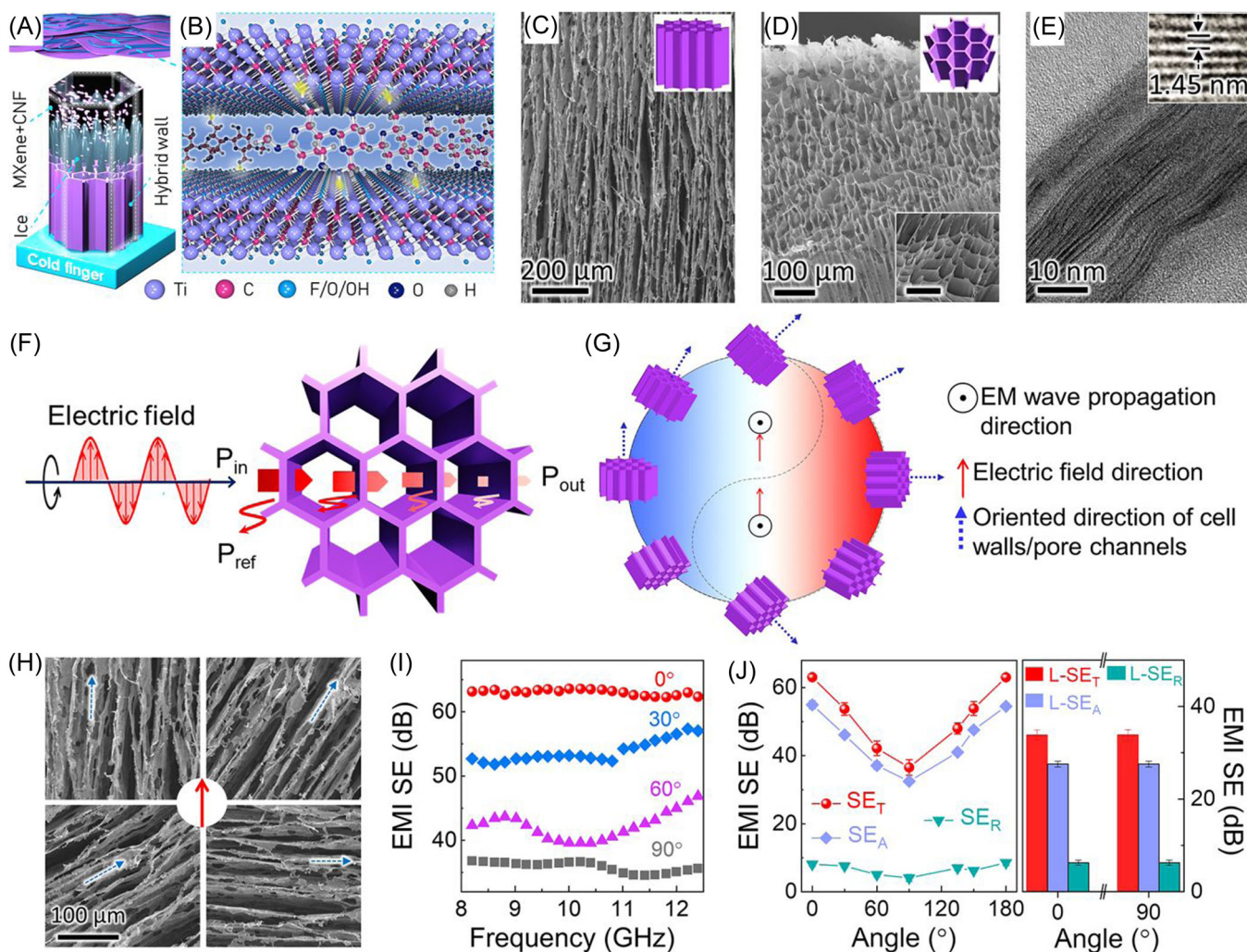
FIGURE 9 (A) Schematic of the assembled metal carbides/nitride (MXene)/cellulose nanofibril (CNF) hybrid cell walls and the unidirectional freezing process of the MXene/CNF-mixed dispersion. (B) Schematic of the MXene, the CNFs, and their noncovalent interactions. Scanning electron microscopy (SEM) image of the (C) longitudinal plane and (D) transverse plane for the MXene/CNF hybrid aerogels with 17 wt% CNF and density of 4 mg/cm^3. (E) Cross-sectional transmission electron microscope (TEM) images of the corresponding MXene/CNF hybrid cell walls. (F) The electromagnetic interference (EMI) shielding mechanism when the incident EM waves propagate in the transverse direction, showing the most multiple reflections of EM waves in this direction. (G) Corresponding cell walls'/pore channels' orientation-induced EMI shielding mechanism, which is reflected by the Yin-Yang symbol that represents giving birth to or controlling everything in ancient China. Herein, the blue and red regions in the symbol correspond to angles with a smaller and larger transmission of the incident EM waves, respectively. (H) SEM images of the MXene/CNF hybrid aerogels with various angles (0°, 30°, 60°, and 90°) between the oriented direction of the cell walls and the electric field direction of incident EMWs. (I) EMI SE of the MXene/CNF hybrid aerogels with CNF content of 17 wt% and density of 4 mg/cm^3 at various angles between the oriented direction of the cell walls and electric field direction of incident EMWs, and the angle-induced. (J) Transverse (SE_T, SE_A, and SE_R) and longitudinal (L-SE_T, L-SE_A, and L-SE_R) EMI shielding performance change at 10 GHz frequency. Reproduced with permission: Copyright 2020, Wiley.[46]

shielding performance. The EMI SE of the composite aerogels reached 74.6 or 35.5 dB at a density of merely 8.0 or 1.5 mg/cm^3, respectively. The SSE/t was up to 189,400 dB·cm^2/g, significantly exceeding most other EMI shielding materials. CNF was also efficiently employed as a green dispersant, cross-linker, and structure-directing agent, assisting in the preparation of large-area ambient pressure dried CNT aerogels via a facile, energy-efficient, and scalable freezing–thawing–drying approach. The resultant composite aerogels showed unidirectional micro-honeycomb pore channels, high mechanical strength, good conductivity, and controllable, wide-range densities. Adjusting the angle of the pore orientation with respect to the electric field direction of the incident EMWs was further demonstrated to facilely control the EMI shielding performance of the composite aerogels.

5 | CONCLUSION AND OUTLOOK

In this review, different kinds of versatile nanomaterials have been explored and they are integrated with nanocellulose to fabricate composite films or aerogels for high-performance EMI shields has been reviewed. The composition structures have proved to have a significant influence on the performance of composite films, which can be traced back to the controlled assembly method. The double- or alternating-layer structure ensures a high-purity conducting layer to enhance the EMI SE, while the strong interfacial interaction in "brick-and-mortar" structure also improves the mechanical strength and toughness. Moreover, the introduction of porous structure in the nanocomposites not only reduces the weight significantly but also introduces more multiple reflections of incident EMWs, contributing to higher EMI shielding performance. Particularly, the pore shapes including random and aligned pore morphologies of the nanocellulose-based EMI shields have been discussed, showing a remarkable influence on the EMI shielding performance. The design of the porous structure is a promising and effective way to optimize the EMI shielding performance for the nanocellulose-based composite foams.

Rational design and controllable assembly of the nanocellulose-based EMI shielding architectures for achieving high EMI shielding performance are already in the research focus. However, it remains challenging to prepare the EMI shields in a low-cost, energy-efficiency, and scalable approach to advance the practical applications. Developing more facile approaches to achieve high-efficiency utilization of the functional nanomaterials, nanocellulose, and microstructure for improving the EMI shielding performance as well as to promote the understanding of the structure–property relationships is highly desired. Moreover, minimizing the material consumption, that is, reducing the density and thickness, while retaining high EMI SE and good mechanical properties is of critical importance for next-generation EMI shielding architectures, and the nanocellulose-based EMI shields showcase the high potential for achieving lightweight, high EMI shielding performance. Meanwhile, integrating multifunctionalities into the nanocellulose-based EMI shields for intelligent electronics is emerging and is required in future electronic appliances, especially for the development of the Internet of Things. In summary, the nanocellulose with environmental friendliness, sustainability, renewability, excellent mechanical properties, and unique structure characteristics offers promising prospects for preparing high-performance EMI shields.

CONFLICTS OF INTEREST

The authors declare no conflicts of interest.

ORCID

Gustav Nyström 🄳 http://orcid.org/0000-0003-2739-3222

REFERENCES

1. Cao MS, Cai YZ, He P, Shu JC, Cao WQ, Yuan J. 2D MXenes: electromagnetic property for microwave absorption and electromagnetic interference shielding. *Chem Eng J.* 2019; 359:1265-1302.
2. Thomassin JM, Jerome C, Pardoen T, Bailly C, Huynen I, Detrembleur C. Polymer/carbon based composites as electromagnetic interference (EMI) shielding materials. *Mater Sci Eng R.* 2013;74(7):211-232.
3. Chang C, Yue X, Hao B, Xing D, Ma PC. Direct growth of carbon nanotubes on basalt fiber for the application of electromagnetic interference shielding. *Carbon.* 2020;167:31-39.
4. Liu P, Gao S, Zhang G, Huang Y, You W, Che R. Hollow engineering to Co@N-doped carbon nanocages via synergistic protecting-etching strategy for ultrahigh microwave absorption. *Adv Funct Mater.* 2021;31(27):2102812.
5. Esfahani AN, Katbab A, Taeb A, Simon L, Pope MA. Correlation between mechanical dissipation and improved X-band electromagnetic shielding capabilities of amine functionalized graphene/thermoplastic polyurethane composites. *Eur Polym J.* 2017;95:520-538.
6. Cao W, Ma C, Tan S, Ma M, Wan P, Chen F. Ultrathin and flexible CNTs/MXene/cellulose nanofibrils composite paper for electromagnetic interference shielding. *Nano-Micro Lett.* 2019;11(1):72.
7. Yang R, Gui X, Yao L, et al. Ultrathin, lightweight, and flexible CNT buckypaper enhanced using MXenes for electromagnetic interference shielding. *Nano-Micro Lett.* 2021;13(1):66.
8. Wang M, Tang XH, Cai JH, Wu H, Shen JB, Guo SY. Fabrication, mechanisms and perspectives of conductive polymer composites with multiple interfaces for electromagnetic interference shielding: a review. *Carbon.* 2021;177:377-402.
9. Iqbal A, Sambyal P, Koo CM. 2D MXenes for electromagnetic shielding: a review. *Adv Funct Mater.* 2020;30(47):2000883.
10. Chen Y, Yang Y, Xiong Y, et al. Porous aerogel and sponge composites: assisted by novel nanomaterials for electromagnetic interference shielding. *Nano Today.* 2021;38: 101204.
11. Zeng Z, Chen M, Jin H, et al. Thin and flexible multi-walled carbon nanotube/waterborne polyurethane composites with high-performance electromagnetic interference shielding. *Carbon.* 2016;96:768-777.

12. Zeng Z, Jin H, Chen M, Li W, Zhou L, Zhang Z. Lightweight and anisotropic porous MWCNT/WPU composites for ultrahigh performance electromagnetic interference shielding. *Adv Funct Mater.* 2016;26(2):303-310.

13. Huangfu Y, Ruan K, Qiu H, et al. Fabrication and investigation on the PANI/MWCNT/thermally annealed graphene aerogel/epoxy electromagnetic interference shielding nanocomposites. *Compos Part A.* 2019;121:265-272.

14. Angappan M, Bora PJ, Vinoy KJ, Ramamurthy PC, Vijayaraju K. Tailorable electromagnetic interference shielding using nickel coated glass fabric-epoxy composite with excellent mechanical property. *Compos Commun.*2018;10:110-115.

15. Han M, Shuck CE, Rakhmanov R, et al. Beyond $Ti_3C_2T_x$: MXenes for electromagnetic interference shielding. *ACS Nano.* 2020;14(4):5008-5016.

16. Yang W, Liu JJ, Wang LL, et al. Multifunctional MXene/ natural rubber composite films with exceptional flexibility and durability. *Compos B Eng.*2020;188:107875.

17. Wang L, Shi X, Zhang J, Zhang Y, Gu J. Lightweight and robust rGO/sugarcane derived hybrid carbon foams with outstanding EMI shielding performance. *J Mater Sci Technol.* 2020;52:119-126.

18. Kumar R, Sahoo S, Joanni E, et al. Recent progress on carbon-based composite materials for microwave electromagnetic interference shielding. *Carbon.* 2021;177:304-331.

19. Wu N, Hu Q, Wei R, et al. Review on the electromagnetic interference shielding properties of carbon based materials and their novel composites: recent progress, challenges and prospects. *Carbon.* 2021;176:88-105.

20. Liu H, Wu S, You C, Tian N, Li Y, Chopra N. Recent progress in morphological engineering of carbon materials for electromagnetic interference shielding. *Carbon.* 2021;172: 569-596.

21. Wang YY, Zhou ZH, Zhou CG, et al. Lightweight and robust carbon nanotube/polyimide foam for efficient and heat-resistant electromagnetic interference shielding and microwave absorption. *ACS Appl Mater Interfaces.* 2020;12(7): 8704-8712.

22. Hu P, Lyu J, Fu C, et al. Multifunctional aramid nanofiber/ carbon nanotube hybrid aerogel films. *ACS Nano.* 2020;14(1): 688-697.

23. Cai JH, Li J, Chen XD, Wang M. Multifunctional poly-dimethylsiloxane foam with multi-walled carbon nanotube and thermo-expandable microsphere for temperature sensing microwave shielding and piezoresistive sensor. *Chem Eng J.* 2020;393:124805.

24. Wang Z, Kong QQ, Yi ZL, et al. Electromagnetic interference shielding material for super-broadband: multi-walled carbon nanotube/silver nanowire film with an ultrathin sandwich structure. *J Mater Chem A.* 2021;9(46):25999-26009.

25. Sun Z, Chen J, Jia X, Wang G, Shen B, Zheng W. Humidification of high-performance and multifunctional polyimide/carbon nanotube composite foams for enhanced electromagnetic shielding. *Mater Today Phys.* 2021;21: 100521.

26. Fei Y, Chen F, Fang W, et al. High-strength flexible and cycling-stable piezo-resistive polymeric foams derived from thermoplastic polyurethane and multi-wall carbon nano-tubes. *Compos B Eng.*2020;199:108279.

27. Fei Y, Chen F, Fang W, et al. Conductive thermoplastic polyurethane nanocomposite foams derived from a cellulose/ MWCNTs aerogel framework: simultaneous enhancement of piezoresistance strength and endurance. *J Mater Chem C.* 2021;9(38):13103-13114.

28. Gupta S, Tai NH. Carbon materials and their composites for electromagnetic interference shielding effectiveness in X-band. *Carbon.* 2019;152:159-187.

29. Song P, Liu B, Liang C, et al. Lightweight flexible cellulose-derived carbon aerogel@reduced graphene oxide/PDMS composites with outstanding EMI shielding performances and excellent thermal conductivities. *Nano-Micro Lett.*2021; 13(1):91.

30. Yin X, Li H, Han L, et al. Lightweight and flexible 3D graphene microtubes membrane for high-efficiency electromagnetic-interference shielding. *Chem Eng J.* 2020; 387:124025.

31. Liang L, Xu P, Wang Y, et al. Flexible polyvinylidene fluoride film with alternating oriented graphene/Ni nanochains for electromagnetic interference shielding and thermal management. *Chem Eng J.* 2020;395:125209.

32. Liang C, Hamidinejad M, Ma L, Wang Z, Park CB. Lightweight and flexible graphene/SiC-nanowires/poly (vinylidene fluoride) composites for electromagnetic interference shielding and thermal management. *Carbon.* 2020; 156:58-66.

33. Gao W, Zhao N, Yu T, et al. High-efficiency electromagnetic interference shielding realized in nacre-mimetic graphene/ polymer composite with extremely low graphene loading. *Carbon.* 2020;157:570-577.

34. Huang B, Liu X, Tan L, et al. Superior electromagnetic interference shielding 3D graphene nanoplatelets/reduced graphene oxide foam/epoxy nanocomposites with high thermal conductivity. *J Mater Chem C.* 2019;7(9):2725-2733.

35. Liao Y, Duan F, Zhang H, et al. Ultrafast response of spray-on nanocomposite piezoresistive sensors to broadband ultrasound. *Carbon.* 2019;143:743-751.

36. Chen Y, Zhang HB, Huang Y, Jiang Y, Zheng WG, Yu ZZ. Magnetic and electrically conductive epoxy/graphene/car-bonyl iron nanocomposites for efficient electromagnetic interference shielding. *Compos Sci Technol.* 2015;118: 178-185.

37. Gao L, Li C, Huang W, et al. MXene/polymer membranes: synthesis properties and emerging applications. *Chem Mater.* 2020;32(5):1703-1747.

38. Jin X, Wang J, Dai L, et al. Flame-retardant poly(vinyl alcohol)/MXene multilayered films with outstanding electromagnetic interference shielding and thermal conductive performances. *Chem Eng J.* 2020;380:122475.

39. Gao Q, Pan Y, Zheng G, Liu C, Shen C, Liu X. Flexible multilayered MXene/thermoplastic polyurethane films with excellent electromagnetic interference shielding thermal conductivity and management performances. *Adv Compos Hybrid Mater.* 2021;4(2):274-285.

40. Lu J, Zhang Y, Tao Y, et al. Self-healable castor oil-based waterborne polyurethane/MXene film with outstanding electromagnetic interference shielding effectiveness and excellent shape memory performance. *J Colloid Interface Sci.* 2021;588:164-174.

41. Song P, Liu B, Qiu H, Shi X, Cao D, Gu J. MXenes for polymer matrix electromagnetic interference shielding composites: a review. *Compos Commun.* 2021;24:100653.

42. Xu H, Yin X, Li X, et al. Lightweight Ti_2CT_x MXene/poly (vinyl alcohol) composite foams for electromagnetic wave shielding with absorption-dominated feature. *ACS Appl Mater Interfaces.* 2019;11(10):10198-10207.

43. Ma W, Cai W, Chen W, Liu P, Wang J, Liu Z. A novel structural design of shielding capsule to prepare high-performance and self-healing MXene-based sponge for ultra-efficient electromagnetic interference shielding. *Chem Eng J.* 2021;426:130729.

44. Li Y, Chen Y, Liu Y, Zhang C, Qi H. Holocellulose nanofibrils assisted exfoliation to prepare MXene-based composite film with excellent electromagnetic interference shielding performance. *Carbohydr Polym.* 2021;274:118652.

45. Jiang Y, Ru X, Che W, et al. Flexible mechanically robust and self-extinguishing MXene/wood composite for efficient electromagnetic interference shielding. *Compos B Eng.* 2022;229:109460.

46. Zeng Z, Wang C, Siqueira G, et al. Nanocellulose-MXene biomimetic aerogels with orientation-tunable electromagnetic interference shielding performance. *Adv Sci.* 2020;7(15):2000979.

47. Chen W, Liu LX, Zhang HB, Yu ZZ. Kirigami-inspired highly stretchable conductive and hierarchical $Ti_3C_2T_x$ MXene films for efficient electromagnetic interference shielding and pressure sensing. *ACS Nano.* 2021;15(4):7668-7681.

48. Luo JQ, Zhao S, Zhang HB, Deng Z, Li L, Yu ZZ. Flexible stretchable and electrically conductive MXene/natural rubber nanocomposite films for efficient electromagnetic interference shielding. *Compos Sci Technol.* 2019;182:107754.

49. Qian K, Zhou Q, Wu H, et al. Carbonized cellulose microsphere@void@MXene composite films with egg-box structure for electromagnetic interference shielding. *Compos Part A.* 2021;141:106229.

50. Zhao S, Zhang HB, Luo JQ, et al. Highly electrically conductive three-dimensional $Ti_3C_2T_x$ MXene/reduced graphene oxide hybrid aerogels with excellent electromagnetic interference shielding performances. *ACS Nano.* 2018;12(11):11193-11202.

51. Gao J, Luo J, Wang L, et al. Flexible superhydrophobic and highly conductive composite based on non-woven polypropylene fabric for electromagnetic interference shielding. *Chem Eng J.* 2019;364:493-502.

52. Li TT, Wang Y, Peng HK, et al. Lightweight flexible and superhydrophobic composite nanofiber films inspired by nacre for highly electromagnetic interference shielding. *Compos Part A.* 2020;128:105685.

53. Bansala T, Mukhopadhyay S, Joshi M, Doong Ra, Chaudhary M. Synthesis and shielding properties of PVP-stabilized-AgNPs-based graphene nanohybrid in the Ku band. *Synth Met.* 2016;221:86-94.

54. Xu J, Jiang S, Peng L, et al. AgNps-PVA-coated woven cotton fabric: preparation water repellency shielding properties and antibacterial activity. *J Ind Text.* 2019;48(10):1545-1565.

55. Fan Z, Di L, Bu D, Zhang T, Zhang X. In-situ reduction of silver by surface DBD plasma: a novel method for preparing highly effective electromagnetic interference shielding Ag/PET. *Plasma Sci Technol.* 2021;23(3):035502.

56. Merizgui T, Gaoui B, Sebaey TA, Prakash VRA. Electromagnetic shielding behavior of epoxy multi-hybrid composites comprises of E-glass fiber Ag nanoparticle and Ni nanosheet: a novel approach. *Polym Compos.* 2021;42(5):2484-2491.

57. Gao Q, Qin J, Guo B, et al. High-performance electromagnetic interference shielding epoxy/Ag nanowire/thermal annealed graphene aerogel composite with bicontinuous three-dimensional conductive skeleton. *Compos Part A.* 2021;151:106648.

58. Chen Y, Pang L, Li Y, et al. Ultra-thin and highly flexible cellulose nanofiber/silver nanowire conductive paper for effective electromagnetic interference shielding. *Compos Part A.* 2020;135:105960.

59. Huang HD, Liu CY, Zhang LQ, Zhong GJ, Li ZM. Simultaneous reinforcement and toughening of carbon nanotube/cellulose conductive nanocomposite films by interfacial hydrogen bonding. *ACS Sustainable Chem Eng.* 2015;3(2):317-324.

60. Liao SY, Wang XY, Li XM, et al. Flexible liquid metal/cellulose nanofiber composites film with excellent thermal reliability for highly efficient and broadband EMI shielding. *Chem Eng J.* 2021;422:129962.

61. Panda S, Acharya B. PDMS/MWCNT nanocomposites as capacitive pressure sensor and electromagnetic interference shielding materials. *J Mater Sci.* 2021;32(12):16215-16229.

62. Liu R, Wang D, Xie Y, Li J, Wang L. Flexible cellulose-based material with a higher conductivity and electromagnetic shielding performance from electroless nickel plating. *Wood Sci Technol.* 2021;55(6):1693-1710.

63. Zeng ZH, Wu N, Wei JJ, et al. Porous and ultra-flexible crosslinked MXene/polyimide composites for multifunctional electromagnetic interference shielding. *Nano-Micro Lett.* 2022;14(1):59.

64. Yuan M, Fei Y, Zhang H, et al. Electromagnetic asymmetric films comprise metal organic frameworks derived porous carbon for absorption-dominated electromagnetic interference shielding. *Compos B Eng.* 2022;233:109622.

65. Qiao J, Zhang X, Liu C, et al. Non-magnetic bimetallic MOF-derived porous carbon-wrapped TiO_2/$ZrTiO_4$ composites for efficient electromagnetic wave absorption. *Nano-Micro Lett.* 2021;13(1):75.

66. Liu C, Liao X. Collagen Fiber/Fe_3O_4/polypyrrole nanocomposites for absorption-type electromagnetic interference shielding and radar stealth. *ACS Appl Nano Mater.* 2020;3(12):11906-11915.

67. Gao H, Wang C, Yang Z, Zhang Y. 3D porous nickel metal foam/polyaniline heterostructure with excellent electromagnetic interference shielding capability and superior absorption based on pre-constructed macroscopic conductive framework. *Compos Sci Technol.* 2021;213:108896.

68. Ma Z, Li J, Zhang J, et al. Ultrathin flexible and high-strength Ni/Cu/metallic glass/Cu/Ni composite with alternate magneto-electric structures for electromagnetic shielding. *J Mater Sci Technol.* 2021;81:43-50.

69. Yadav R, Jamatia T, Kuřitka I, et al. Superparamagnetic $ZnFe_2O_4$ nanoparticles-reduced graphene oxide-polyurethane resin based nanocomposites for electromagnetic interference shielding application. *Nanomaterials.* 2021;11(5):1112.

70. Zeng Z, Wu T, Han D, Ren Q, Siqueira G, Nystrom G. Ultralight flexible and biomimetic nanocellulose/silver nanowire aerogels for electromagnetic interference shielding. *ACS Nano*. 2020;14(3):2927-2938.

71. Zeng Z, Wang C, Wu T, et al. Nanocellulose assisted preparation of ambient dried large-scale and mechanically robust carbon nanotube foams for electromagnetic interference shielding. *J Mater Chem A*. 2020;8(35):17969-17979.

72. Zeng Z, Mavrona E, Sacré D, et al. Terahertz birefringent biomimetic aerogels based on cellulose nanofibers and conductive nanomaterials. *ACS Nano*. 2021;15:7451-7462.

73. Han G, Ma Z, Zhou B, et al. Cellulose-based Ni-decorated graphene magnetic film for electromagnetic interference shielding. *J Colloid Interface Sci*. 2021;583:571-578.

74. Chen Y, Potschke P, Pionteck J, Voit B, Qi H. Multifunctional cellulose/rGO/Fe$_3$O$_4$ composite aerogels for electromagnetic interference shielding. *ACS Appl Mater Interfaces*. 2020;12(19): 22088-22098.

75. Liu J, Zhang HB, Sun R, et al. Hydrophobic flexible and lightweight MXene foams for high-performance electromagnetic-interference shielding. *Adv Mater*. 2017;29(38):1702367.

76. Ameli A, Jung PU, Park CB. Electrical properties and electromagnetic interference shielding effectiveness of polypropylene/carbon fiber composite foams. *Carbon*. 2013;60:379-391.

77. Han M, Yin X, Hantanasirisakul K, et al. Anisotropic MXene aerogels with a mechanically tunable ratio of electromagnetic wave reflection to absorption. *Adv Opt Mater*. 2019;7(10):1900267.

78. Li M, Han F, Jiang S, et al. Lightweight cellulose nanofibril/reduced graphene oxide aerogels with unidirectional pores for efficient electromagnetic interference shielding. *Adv Mater Interfaces*. 2021;8(24):2101437.

79. Zeng Z, Jin H, Chen M, et al. Microstructure design of lightweight flexible and high electromagnetic shielding porous multiwalled carbon nanotube/polymer composites. *Small*. 2017;13(34):1701388.

80. Zeng Z, Wang C, Zhang Y, et al. Ultralight and highly elastic graphene/lignin-derived carbon nanocomposite aerogels with ultrahigh electromagnetic interference shielding performance. *ACS Appl Mater Interfaces*. 2018;10(9):8205-8213.

81. Kaushik M, Moores A. Review: nanocelluloses as versatile supports for metal nanoparticles and their applications in catalysis. *Green Chem*. 2016;18(3):622-637.

82. Ahankari SS, Subhedar AR, Bhadauria SS, Dufresne A. Nanocellulose in food packaging: a review. *Carbohydr Polym*. 2021;255:117479.

83. Chen W, Yu H, Lee SY, Wei T, Li J, Fan Z. Nanocellulose: a promising nanomaterial for advanced electrochemical energy storage. *Chem Soc Rev*. 2018;47(8):2837-2872.

84. Hu B, Pu H, Sun DW. Multifunctional cellulose based substrates for SERS smart sensing: principles applications and emerging trends for food safety detection. *Trends Food Sci Technol*. 2021;110:304-320.

85. Zhang X, Zhao X, Xue T, Yang F, Fan W, Liu T. Bidirectional anisotropic polyimide/bacterial cellulose aerogels by freeze-drying for super-thermal insulation. *Chem Eng J*. 2020;385: 123963.

86. Guan H, Cheng Z, Wang X. Highly compressible wood sponges with a spring-like lamellar structure as effective and reusable oil absorbents. *ACS Nano*. 2018;12(10):10365-10373.

87. Chen Y, Zhang L, Yang Y, et al. Recent progress on nanocellulose aerogels: preparation modification composite fabrication applications. *Adv Mater*. 2021;33(11):2005569.

88. Li T, Chen C, Brozena AH, et al. Developing fibrillated cellulose as a sustainable technological material. *Nature*. 2021;590(7844):47-56.

89. De France K, Zeng ZH, Wu TT, Nyström G. Functional materials from nanocellulose: utilizing structure–property relationships in bottom-up fabrication. *Adv Mater*. 2021;33(28):2000657.

90. Yu HY, Zhang DZ, Lu FF, Yao JM. New approach for single-step extraction of carboxylated cellulose nanocrystals for their use As adsorbents and flocculants. *ACS Sustainable Chem Eng*. 2016;4(5):2632-2643.

91. Chen LH, Zhu JY, Baez C, Kitin P, Elder T. Highly thermal-stable and functional cellulose nanocrystals and nanofibrils produced using fully recyclable organic acids. *Green Chem*. 2016;18(13):3835-3843.

92. Leung AC, Hrapovic S, Lam E, et al. Characteristics and properties of carboxylated cellulose nanocrystals prepared from a novel one-step procedure. *Small*. 2011;7(3):302-305.

93. Espinosa SC, Kuhnt T, Foster EJ, Weder C. Isolation of thermally stable cellulose nanocrystals by phosphoric acid hydrolysis. *Biomacromolecules*. 2013;14(4):1223-1230.

94. Li QQ, Renneckar S. Supramolecular structure characterization of molecularly thin cellulose I nanoparticles. *Biomacromolecules*. 2011;12(3):650-659.

95. Jarvis M. Chemistry-cellulose stacks up. *Nature*. 2003; 426(6967):611-612.

96. Chen WS, Yu HP, Li Q, Liu YX, Li J. Ultralight and highly flexible aerogels with long cellulose I nanofibers. *Soft Matter*. 2011;7(21):10360-10368.

97. Zheng QF, Cai ZY, Gong SQ. Green synthesis of polyvinyl alcohol (PVA)-cellulose nanofibril (CNF) hybrid aerogels and their use as superabsorbents. *J Mater Chem A*. 2014;2(9): 3110-3118.

98. Javadi A, Zheng Q, Payen F, et al. Polyvinyl alcohol-cellulose nanofibrils-graphene oxide hybrid organic aerogels. *ACS App Mater Interfaces*. 2013;5(13):5969-5975.

99. Xiao S, Chen C, Xia Q, et al. Lightweight strong moldable wood via cell wall engineering as a sustainable structural material. *Science*. 2021;374(6566):465-471.

100. Kontturi E, Laaksonen P, Linder MB, et al. Advanced materials through assembly of nanocelluloses. *Adv Mater*. 2018;30(24):1703779.

101. Moon RJ, Martini A, Nairn J, Simonsen J, Youngblood J. Cellulose nanomaterials review: structure properties and nanocomposites. *Chem Soc Rev*. 2011;40(7):3941-3994.

102. Habibi Y, Lucia LA, Rojas OJ. Cellulose nanocrystals: chemistry self-assembly and applications. *Chem Rev*. 2010; 110(6):3479-3500.

103. Klemm D, Kramer F, Moritz S, et al. Nanocelluloses: a new family of nature-based materials. *Angew Chem Int Ed*. 2011; 50(24):5438-5466.

104. Shatkin JA, Wegner TH, Bilek EM, Cowie J. Market projections of cellulose nanomaterial-enabled products— Part 1: applications. *Tappi J*. 2014;13(5):9-16.

105. Domingues RMA, Gomes ME, Reis RL. The potential of cellulose nanocrystals in tissue engineering strategies. *Biomacromolecules*. 2014;15(7):2327-2346.

106. Foster EJ, Moon RJ, Agarwal UP, et al. Current characterization methods for cellulose nanomaterials. *Chem Soc Rev.* 2018;47(8):2609-2679.

107. De France KJ, Cranston ED, Hoare T. Mechanically reinforced injectable hydrogels. *ACS Appl Polym Mater.* 2020;2(3):1016-1030.

108. Habibi Y. Key advances in the chemical modification of nanocelluloses. *Chem Soc Rev.* 2014;43(5):1519-1542.

109. Lin N, Dufresne A. Nanocellulose in biomedicine: current status and future prospect. *Eur Polym J.* 2014;59:302-325.

110. Cowie J, Bilek EM, Wegner TH, Shatkin JA. Market projections of cellulose nanomaterial-enabled products—Part 2: volume estimates. *Tappi J.* 2014;13(6):57-69.

111. Mariano M, El Kissi N, Dufresne A. Cellulose nanocrystals and related nanocomposites: review of some properties and challenges. *J Polym Sci B.* 2014;52(12):791-806.

112. Moon RJ, Schueneman GT, Simonsen J. Overview of cellulose nanomaterials their capabilities and applications. *JOM.* 2016;68(9):2383-2394.

113. Dugan JM, Gough JE, Eichhorn SJ. Bacterial cellulose scaffolds and cellulose nanowhiskers for tissue engineering. *Nanomedicine.* 2013;8(2):287-298.

114. Plackett DV, Letchford K, Jackson JK, Burt HM. A review of nanocellulose as a novel vehicle for drug delivery. *Nord Pulp Pap Res J.* 2014;29(1):105-118.

115. Jorfi M, Foster EJ. Recent advances in nanocellulose for biomedical applications. *J Appl Polym Sci.* 2015;132(14):41719.

116. Beck-Candanedo S, Roman M, Gray DG. Effect of reaction conditions on the properties and behavior of wood cellulose nanocrystal suspensions. *Biomacromolecules.* 2005;6(2):1048-1054.

117. Li Y, Xue B, Yang S, Cheng Z, Xie L, Zheng Q. Flexible multilayered films consisting of alternating nanofibrillated cellulose/Fe_3O_4 and carbon nanotube/polyethylene oxide layers for electromagnetic interference shielding. *Chem Eng J.* 2021;410:128356.

118. Wu N, Zeng Z, Kummer N, Han D, Zenobi R, Nyström G. Ultrafine cellulose nanofiber-assisted physical and chemical cross-linking of MXene sheets for electromagnetic interference shielding. *Small Methods.*2021;5(12):2100889.

119. Zhou Z, Song Q, Huang B, Feng S, Lu C. Facile fabrication of densely packed Ti_3C_2 MXene/nanocellulose composite films for enhancing electromagnetic interference shielding and electro-/photothermal performance. *ACS Nano.* 2021;15(7):12405-12417.

120. Liang C, Gu Z, Zhang Y, Ma Z, Qiu H, Gu J. Structural design strategies of polymer matrix composites for electromagnetic interference shielding: a review. *Nano-Micro Lett.*2021;13(1):181.

121. Wan YJ, Li XM, Zhu PL, Sun R, Wong CP, Liao WH. Lightweight flexible MXene/polymer film with simultaneously excellent mechanical property and high-performance electromagnetic interference shielding. *Compos Part A.* 2020;130:105764.

122. Thostenson ET, Chou TW. Processing materials with microwave energy. *Mater Sci Eng A.* 2000;287:153-158.

123. Kamkar M, Ghaffarkhah A, Hosseini E, Amini M, Ghaderi S, Arjmand M. Multilayer polymeric nanocomposites for electromagnetic interference shielding: fabrication mechanisms and prospects. *New J Chem.* 2021;45(46):21488-21507.

124. Ohlan A, Singh K, Chandra A, Dhawan SK. Microwave absorption behavior of core-shell structured poly (3,4-ethylenedioxy thiophene)-barium ferrite nanocomposites. *ACS Appl Mater Interfaces.* 2010;2(3):927-933.

125. Peng M, Qin F. Clarification of basic concepts for electromagnetic interference shielding effectiveness. *J Appl Phys.* 2021;130(22):225108.

126. Shahzad F, Alhabeb M, Hatter CB, et al. Electromagnetic interference shielding with 2D transition metal carbides (MXenes). *Science.* 2016;353(6304):1137-1140.

127. Simon RM. Emi shielding through conductive plastics. *Polym Plast Technol Eng.* 1981;17(1):1-10.

128. Zeng Z, Jiang F, Yue Y, et al. Flexible and ultrathin waterproof cellular membranes based on high-conjunction metal-wrapped polymer nanofibers for electromagnetic interference shielding. *Adv Mater.* 2020;32:1908496.

129. Cao WT, Chen FF, Zhu YJ, et al. Binary strengthening and toughening of MXene/cellulose nanofiber composite paper with nacre-inspired structure and superior electromagnetic interference shielding properties. *ACS Nano.* 2018;12(5):4583-4593.

130. Xu W, Wang GS, Yin PG. Designed fabrication of reduced graphene oxides/Ni hybrids for effective electromagnetic absorption and shielding. *Carbon.* 2018;139:759-767.

131. Mural PK, Pawar SP, Jayanthi S, Madras G, Sood AK, Bose S. Engineering nanostructures by decorating magnetic nanoparticles onto graphene oxide sheets to shield electromagnetic radiations. *ACS Appl Mater Interfaces.* 2015;7(30):16266-16278.

132. Parit M, Du H, Zhang X, Prather C, Adams M, Jiang Z. Polypyrrole and cellulose nanofiber based composite films with improved physical and electrical properties for electromagnetic shielding applications. *Carbohydr Polym.* 2020;240:116304.

133. Cui C, Xiang C, Geng L, et al. Flexible and ultrathin electrospun regenerate cellulose nanofibers and d-$Ti_3C_2T_x$ (MXene) composite film for electromagnetic interference shielding. *J Alloys Compd.* 2019;788:1246-1255.

134. Li L, Ma Z, Xu P, et al. Flexible and alternant-layered cellulose nanofiber/graphene film with superior thermal conductivity and efficient electromagnetic interference shielding. *Compos Part A.* 2020;139:106134.

135. Zhou B, Zhang Z, Li Y, et al. Flexible robust and multifunctional electromagnetic interference shielding film with alternating cellulose nanofiber and MXene layers. *ACS Appl Mater Interfaces.* 2020;12(4):4895-4905.

136. Zhan Z, Song Q, Zhou Z, Lu C. Ultrastrong and conductive MXene/cellulose nanofiber films enhanced by hierarchical nano-architecture and interfacial interaction for flexible electromagnetic interference shielding. *J Mater Chem C.* 2019;7(32):9820-9829.

137. Xu X, Wu S, Cui J, et al. Insights into the microstructures and reinforcement mechanism of nano-fibrillated cellulose/MXene based electromagnetic interference shielding film. *Cellulose.* 2021;28(6):3311-3325.

138. Cui Z, Gao C, Fan Z, et al. Lightweight MXene/cellulose nanofiber composite film for electromagnetic interference shielding. *J Electron Mater.* 2021;50(4):2101-2110.

139. Liu Q, Zhang Y, Liu Y, Liu Z, Zhang B, Zhang Q. Ultrathin biomimetic multifunctional leaf-like silver nanowires/

Ti$_3$C$_2$T$_x$ MXene/cellulose nanofibrils nanocomposite film for high-performance electromagnetic interference shielding and thermal management. *J Alloys Compd*. 2021;860:158151.

140. Yang W, Zhao Z, Wu K, et al. Ultrathin flexible reduced graphene oxide/cellulose nanofiber composite films with strongly anisotropic thermal conductivity and efficient electromagnetic interference shielding. *J Mater Chem C*. 2017;5(15):3748-3756.

141. Wiemann J, Yang TR, Sander PN, et al. Completely green approach for the preparation of strong and highly conductive graphene composite film by using nanocellulose as dispersing agent and mechanical compression. *ACS Sustainable Chem Eng*. 2017;5(10):9102-9113.

142. Zhang X, Lu Z, Zhao J, Li Q, Zhang W, Lu C. Exfoliation/dispersion of low-temperature expandable graphite in nanocellulose matrix by wet co-milling. *Carbohydr Polym*. 2017;157:1434-1441.

143. Yang W, Gong Y, Zhao X, et al. Strong and highly conductive graphene composite film based on the nanocellulose-assisted dispersion of expanded graphite and incorporation of poly (ethylene oxide). *ACS Sustainable Chem Eng*. 2019;7(5):5045-5056.

144. Lapka T, Kopecký D, Mazúr P, et al. Elaboration and properties of nanofibrillated cellulose composites with polypyrrole nanotubes or their carbonized analogs. *Synth Met*. 2021;278:116806.

145. Zhang H, Sun X, Heng Z, Chen Y, Zou H, Liang M. Robust and flexible cellulose nanofiber/multiwalled carbon nanotube film for high-performance electromagnetic interference shielding. *Ind Eng Chem Res*. 2018;57(50):17152-17160.

146. Gopakumar DA, Pai AR, Pottathara YB, et al. Cellulose nanofiber-based polyaniline flexible papers as sustainable microwave absorbers in the X-band. *ACS Appl Mater Interfaces*. 2018;10(23):20032-20043.

147. Zhang K, Gu X, Dai Q, Yuan B, Yan Y, Guo M. Flexible polyaniline-coated poplar fiber composite membranes with effective electromagnetic shielding performance. *Vacuum*. 2019;170:108990.

148. Luo H, Xie J, Xiong L, Zhu Y, Yang Z, Wan Y. Fabrication of flexible ultra-strong and highly conductive bacterial cellulose-based paper by engineering dispersion of graphene nanosheets. *Compos Part B*2019;162:484-490.

149. Qian K, Wu H, Fang J, et al. Yarn-ball-shaped CNF/MWCNT microspheres intercalating Ti$_3$C$_2$T$_x$ MXene for electromagnetic interference shielding films. *Carbohydr Polym*. 2021;254:117325.

150. Jin K, Xing J, Liu X, et al. Manipulating the assembly of the CNC/RGO composite film for superior electromagnetic interference shielding properties. *J Mater Chem A*. 2021;9(47):26999-27009.

151. Qian K, Zhou Q, Thaiboonrod S, et al. Highly thermally conductive Ti$_3$C$_2$T$_x$/h-BN hybrid films via coulombic assembly for electromagnetic interference shielding. *J Colloid Interface Sci*. 2022;613:488-498.

152. Miao M, Liu R, Thaiboonrod S, et al. Silver nanowires intercalating Ti$_3$C$_2$T$_x$ MXene composite films with excellent flexibility for electromagnetic interference shielding. *J Mater Chem C*. 2020;8(9):3120-3126.

153. Zhou Q, Qian K, Fang J, Miao M, Cao S, Feng X. UV-light modulated Ti$_3$C$_2$T$_x$ MXene/g-C$_3$N$_4$ heterojunction film for

electromagnetic interference shielding. *Compos Part A*. 2020;134:105899.

154. Xu Y, Qian K, Deng D, et al. Electroless deposition of silver nanoparticles on cellulose nanofibrils for electromagnetic interference shielding films. *Carbohydr Polym*. 2020;250:116915.

155. Bian R, He G, Zhi W, Xiang S, Wang T, Cai D. Ultralight MXene-based aerogels with high electromagnetic interference shielding performance. *J Mater Chem C*. 2019;7(3):474-478.

156. Xu Z, Hao H. Electromagnetic interference shielding effectiveness of aluminum foams with different porosity. *J Alloys Compd*. 2014;617:207-213.

157. Wei Q, Pei S, Qian X, et al. Superhigh electromagnetic interference shielding of ultrathin aligned pristine graphene nanosheets film. *Adv Mater*. 2020;32(14):e1907411.

158. Zeng Z, Chen M, Pei Y, et al. Ultralight and flexible polyurethane/silver nanowire nanocomposites with unidirectional pores for highly effective electromagnetic shielding. *ACS Appl Mater Interfaces*. 2017;9(37):32211-32219.

159. Liu J, Liu Z, Zhang HB, et al. Ultrastrong and highly conductive MXene-based films for high-performance electromagnetic interference shielding. *Adv Electron Mater*. 2019;6(1):1901094.

160. Liu J, Liu Y, Zhang HB, Dai Y, Liu Z, Yu ZZ. Superelastic and multifunctional graphene-based aerogels by interfacial reinforcement with graphitized carbon at high temperatures. *Carbon*. 2018;132:95-103.

161. Chen Y, Zhang HB, Wang M, Qian X, Dasari A, Yu ZZ. Phenolic resin-enhanced three-dimensional graphene aerogels and their epoxy nanocomposites with high mechanical and electromagnetic interference shielding performances. *Compos Sci Technol*. 2017;152:254-262.

162. Zhang Y, Yu J, Lu J, Zhu C, Qi D. Facile construction of 2D MXene (Ti$_3$C$_2$T$_x$) based aerogels with effective fire-resistance and electromagnetic interference shielding performance. *J Alloys Compd*. 2021;870:159442.

163. Xin W, Ma MG, Chen F. Silicone-coated MXene/cellulose nanofiber aerogel films with photothermal and Joule heating performances for electromagnetic interference shielding. *ACS Appl Nano Mater*. 2021;4(7):7234-7243.

164. Fei Y, Liang M, Zhou T, Chen Y, Zou H. Unique carbon nanofiber@Co/C aerogel derived bacterial cellulose embedded zeolitic imidazolate frameworks for high-performance electromagnetic interference shielding. *Carbon*. 2020;167:575-584.

165. Chen Y, Zhang L, Mei C, et al. Wood-inspired anisotropic cellulose nanofibril composite sponges for multifunctional applications. *ACS Appl Mater Interfaces*. 2020;12(31):35513-35522.

166. Chen Y, Luo H, Guo H, et al. Anisotropic cellulose nanofibril composite sponges for electromagnetic interference shielding with low reflection loss. *Carbohydr Polym*. 2022;276:118799.

167. Wang L, Song P, Lin CT, Kong J, Gu J. 3D shapeable superior electrically conductive cellulose nanofibers/Ti$_3$C$_2$T$_x$ MXene aerogels/epoxy nanocomposites for promising EMI shielding. *Research*. 2020;2020:4093732.

168. Fei Y, Liang M, Yan L, Chen Y, Zou H. Co/C@cellulose nanofiber aerogel derived from metal-organic frameworks for

highly efficient electromagnetic interference shielding. *Chem Eng J.* 2020;392:124815.

AUTHOR BIOGRAPHIES

Zhihui Zeng received his Ph.D. degree in Materials Science and Engineering from the National Center for Nanoscience and Technology (NCNST), University of Chinese Academy of Sciences, Beijing, China in 2016. Following his work as a postdoctoral research fellow at Nanyang Technological University, Singapore and Swiss Federal Laboratories for Materials Science and Technology (Empa), he currently works in the School of Materials Science and Engineering, Shandong University, Jinan, China. His research interests include the design, fabrication, and application of polymer-based nanocomposites, nanostructured assemblies, and cellular materials.

Jing Qiao received his Ph.D. degree in Materials Science and Engineering from Shandong University, Jinan, China in 2021, and continued his postdoctoral research currently. His research interests include the design, fabrication, and application of electromagnetic functional materials.

Runa Zhang received her Master's degree in chemical Engineering and Technology from Yanshan University in 2020 and is currently working as a research assistant at the School of Materials and Engineering, Shandong University in Jinan, China. Her research interests include the design, manufacture and application of electromagnetic functional materials.

Jiurong Liu obtained his Ph.D. from Osaka University in 2004. Then, he worked as a postdoctoral fellow at UCLA until 2008, before beginning his career as a full professor in materials science at Shandong University. His research interests are the synthesis of hybrid nanomaterials for energy storage and electromagnetic applications.

Gustav Nyström received a Ph.D. in Engineering Physics from Uppsala University in 2012. Following postdoctoral work at KTH Royal Institute of Technology (Stockholm) and ETH Zurich, he is now head of the Cellulose & Wood Materials Laboratory at Empa and a Lecturer at ETH Zurich. He was the recipient of the Gunnar Sundblad Research Foundation's Skills Development Prize (2014) and is a Swiss National Science Foundation Ambizione Fellow (2016). His research aims to develop a new generation of active, renewable, and highly functional biomaterials using cellulose and wood as material resources.